

ERDC/GSL TR-00-5

Geotechnical and  
Structures Laboratory



**US Army Corps  
of Engineers®**  
Engineer Research and  
Development Center

*Strategic Environmental Research and Development Program*

# **Assessment of Microgravimetry for UXO Detection and Discrimination**

Dwain K. Butler

December 2000

The contents of this report are not to be used for advertising, publication, or promotional purposes. Citation of trade names does not constitute an official endorsement or approval of the use of such commercial products.

The findings of this report are not to be construed as an official Department of the Army position, unless so designated by other authorized documents.



PRINTED ON RECYCLED PAPER

# **Assessment of Microgravimetry for UXO Detection and Discrimination**

by Dwain K. Butler

Geotechnical and Structures Laboratory  
U.S. Army Engineer Research and Development Center  
3909 Halls Ferry Road  
Vicksburg, MS 39180-6199

Final report

Approved for public release; distribution is unlimited

Prepared for U.S. Army Corps of Engineers  
Washington, DC 20314-1000

Under SERDP Project No. 1170

# Contents

---

Preface .....	iv
1—Introduction.....	1
Background .....	1
UXO Detection and Discrimination .....	1
Scope of Report.....	3
2—UXO Gravity Model.....	4
Concepts of the Potential Field Methods.....	4
Model for UXO Gravity Response .....	6
UXO Gravity Modeling Program .....	9
3—UXO Prolate Spheroid Model: Gravity Anomaly Calculations.....	11
Bulk Density of Representative Ordnance Items .....	11
Investigation of Gravity Anomalies of Prolate Spheroid Models of UXO .....	12
Gravity Anomalies of Representative Ordnance Items .....	16
Detectability Considerations.....	17
4—Relevant Microgravity Surveys for UXO Detection Considerations .....	20
Background .....	20
Microgravity Survey and Measurement Procedures .....	21
Microgravity Surveys—Case Histories .....	22
Microgravity Survey over an Ordnance Item .....	24
Analysis of Microgravity Survey Results .....	29
5—Summary and Recommendations.....	33
Summary and Conclusions .....	33
Recommendations.....	34
References.....	35
SF 298	

# Preface

---

The work documented in this report was performed during October 1999 through September 2000 and was sponsored by the Strategic Environmental Research and Development Program (SERDP), Washington, DC. The project “Assessment of the Potential for Microgravimetry in Remote Discrimination and Identification of Buried UXO” was SERDP Project No. 1170 and was funded under the SERDP Exploratory Development (SEED) initiative. Mr. Bradley P. Smith was Executive Director, SERDP, and Dr. Jeff Marqusee was Technical Director, SERDP, during this period of this project.

Principal Investigator for this work was Dr. Dwain K. Butler, Senior Research Geophysicist, Geotechnical and Structures Laboratory (GSL), U.S. Army Engineer Research and Development Center (ERDC), Vicksburg, MS.

At the time of publication of this report, Dr. Michael J. O’Connor was Director, GSL, and Dr. James R. Houston was Director of ERDC. Commander of ERDC was COL James S. Weller, EN.

*The contents of this report are not to be used for advertising, publication, or promotional purposes. Citation of trade names does not constitute an official endorsement or approval of the use of such commercial products.*

# 1 Introduction

---

## Background

The cleanup of buried unexploded ordnance (UXO) on military properties (closed, closing, and active) requires UXO location surveys. UXO location is accomplished by geophysical surveys that detect and map surface anomalies of a geophysical parameter, such as the total magnetic field or an electromagnetic field property. Geophysical anomalies associated with UXO result from the contrast in UXO physical properties relative to the host medium. Of course, localized geological features, as well as other buried cultural objects (ordnance scrap, cans, wire, etc.), also represent physical property contrasts and produce geophysical anomalies. Fortunately, for many geological settings, the physical property contrasts between UXO and host medium are large, and UXO detection is not difficult. The major problem that arises is that the geophysical anomalies associated with UXO cannot be readily distinguished or discriminated from anomalies (false alarms) caused by other buried objects. A commonly quoted statistic is that as much as 75 percent of UXO cleanup costs are associated with excavation and disposal of false alarm anomalies.

## UXO Detection and Discrimination

The most frequently used geophysical systems for UXO detection surveys are total field magnetometers (TFM) and “simple” time domain electromagnetic induction (TDEM) instruments. “Simple” TDEM systems loosely refer to systems such as the Geonics EM61 and EM61-HH that measure one or two time windows (channels) from the transient decay signal. Application of these systems by experienced geophysical practitioners during demonstrations at controlled UXO test sites achieve probabilities of detection of UXO in excess of 90 percent (USAEC 1997), although the false alarm rates are still unacceptably high. Generally, for production surveys at large sites, only one of these systems will be deployed. Practitioners generally concede that there is insufficient information content in either TFM or simple TDEM datasets for effective discrimination of UXO anomalies from false alarm anomalies. Acquisition of both TFM and simple TDEM datasets gives some potential for discrimination (Barrow, Khadr, and Nelson 1996; Butler et al. 1998). Systems such as the Naval Research Laboratory Multi-Sensor Towed Array Detection System can acquire very high

resolution TFM and TDEM datasets cost effectively over large areas using ganged sensor systems (McDonald and Robertson 1996).

Other geophysical methods that have been proposed for UXO detection surveys are ground penetrating radar (GPR), frequency domain electromagnetic induction (FDEM) systems, and airborne systems of various types. GPR is not a generally applicable tool or approach for large area UXO detection surveys, and efforts using GPR at UXO demonstrations and live site surveys have been failures. Likewise, efforts to place GPR on booms and airborne platforms have been unsuccessful. However, GPR has applicability and considerable potential for small area UXO discrimination and identification efforts, where the UXO are located by other survey methods (Burr 1999). In general, past attempts at airborne UXO detection surveys have been unsuccessful. Recently, TFM surveys from a helicopter platform at 1.5- to 2.5-m el have shown promise for large area UXO detection surveys, detecting areas of UXO concentration as well as larger individual ordnance items (Gamey and Mahler 1997; Gamey et al. 2000). Multi-frequency FDEM systems have performed well at UXO technology demonstrations and show promise for discrimination and identification (Burr 1999), but these systems are not yet widely in use for production surveys.

Additional approaches demonstrated or considered for UXO detection and discrimination are multi-channel and multi-component TDEM systems, multi-component (vector) magnetometers (Simms et al. 2000), magnetic gradiometers, acoustic/seismic methods, and gravimetry. Like GPR, some of these approaches will likely have very limited applicability to large area detection surveys but may contribute to small area surveys for discrimination. Gravimetry and seismic/acoustic methods, in particular, are likely to have only a very limited, niche role for small area UXO discrimination surveys. Multi-channel, multi-component TDEM systems, and multi-frequency FDEM systems have potential for large area UXO detection surveys, as well as possible near-real-time discrimination, in addition to follow-on, small area discrimination of detected anomalies (Won et al. 1998; Butler et al. 1998; McNeill and Bosnar 1996; Snyder et al. 2000).

If gravity surveys and in particular microgravity surveys (Butler 1980, 1984, 1996) can measure the gravitational anomaly produced by buried UXO, the results can be used to estimate the UXO mass excess (and the actual mass, if the soil density and density contrast is known or can be estimated). *No other approach currently applied to UXO detection and discrimination* directly gives a mass estimate. The induced TFM anomaly is independent of ferrous mass and is determined by the contained ferrous volume, the shell thickness, length-to-diameter ratio, magnetic permeability, and the orientation in the earth's magnetic field (Altshuler 1996; McFee and Das 1990). Joint inversion of TFM and microgravity datasets for a geometrically consistent model could yield mass and volume and thus a density estimate. The density estimate will serve as a UXO discriminant, since the UXO bulk density will be less than that of solid steel but more than that of typical rocks or air- or other fluid-filled containers. Realistically, however, microgravity surveys will have potential only for UXO discrimination and identification with small area surveys of objects located by other methods and likely only for large UXO items.

## Scope of Report

This report documents part of the ongoing efforts to develop forward and inverse modeling tools for UXO, specifically, an analytical forward model solution for the gravity response of a realistic UXO model. A prolate spheroid geometry, which is a special case of a general ellipsoid, is selected as an appropriate, realistic model for most UXO. Some practical considerations for UXO survey applications will be considered, but the primary emphasis is on presenting the details of the analytical model and on discussing UXO response predictions using the model. Also, a limited microgravity measurement program was conducted over a typical ordnance item. The results of the microgravity survey are evaluated and compared to model predictions. Finally, based on the results of the model studies and the microgravity survey, conclusions and recommendations are presented.

## 2 UXO Gravity Model

---

### Concepts of the Potential Field Methods

The total gravitational potential  $U_{TP}(\mathbf{r})$  at a point P on the surface of the earth in which a UXO is buried is  $U_{TP}(\mathbf{r}) = U_{OP}(\mathbf{r}) + U_P(\mathbf{r})$ , where  $U_{OP}(\mathbf{r})$  is the normal earth's gravitational potential at P and  $U_P(\mathbf{r})$  is the anomalous potential at P due to the UXO.  $U_P(\mathbf{r})$  is given by

$$U_P(\mathbf{r}) = -G \iiint_R [\rho(\mathbf{r}_o) / |\mathbf{r} - \mathbf{r}_o|] d^3r_o, \quad (1)$$

where  $G$  is the gravitational constant ( $6.672 \times 10^{-11}$  N-m<sup>2</sup>/kg<sup>2</sup>),  $R$  is the region (volume) of space occupied by the UXO,  $\mathbf{r}$  is the position vector of the point P, and  $\mathbf{r}_o$  is the position vector of a volume element within the region  $R$ , where the density is  $\rho(\mathbf{r}_o)$  (actually the density contrast between the UXO and the surrounding soil). The gravitational force field or the gravitational acceleration of a unit mass at point P is given by

$$\mathbf{g}(\mathbf{r}) = -\nabla U_P(\mathbf{r}), \quad (2)$$

where  $\mathbf{g}$  is the anomalous gravitational acceleration caused by the UXO (superimposed on the gravitational acceleration of the earth).

Similar to the development for the total gravitational potential, the anomalous scalar magnetic (magnetostatic) potential at point P due to the UXO is given by

$$V_P(\mathbf{r}) = -\iiint_R \mathbf{M}(\mathbf{r}_o) \cdot \nabla(1 / |\mathbf{r} - \mathbf{r}_o|) d^3r_o, \quad (3)$$

where  $\mathbf{M}(\mathbf{r}_o)$  is the magnetization (magnetic dipole moment per unit volume from both induced and remnant (permanent) magnetization in the UXO), and the gradient inside the integral is understood to be relative to  $\mathbf{r}_o$  (i.e., the source point). For the buried UXO, the earth's magnetic field is the inducing field for the induced magnetization component of  $\mathbf{M}$ . The magnetic field strength at point P is then given by

$$\mathbf{H}(\mathbf{r}) = -\nabla V_P(\mathbf{r}). \quad (4)$$

The potentials  $U$  and  $V$ , as well as the fields  $\mathbf{g}$  and  $\mathbf{H}$ , satisfy Laplace's equation in source-free space. Also, the components of the fields each satisfy

Laplace's equation in source-free space. For example, the vertical component of gravity  $g_z$  satisfies Laplace's equation, where

$$\mathbf{g}(\mathbf{r}) = i g_x(\mathbf{r}) + j g_y(\mathbf{r}) + k g_z(\mathbf{r}), \quad g_z(\mathbf{r}) = \partial U(\mathbf{r}) / \partial z, \quad \text{and} \quad \nabla^2 g_z = 0, \quad (5)$$

and  $\mathbf{i}, \mathbf{j}, \mathbf{k}$  are unit vectors in a local Cartesian coordinate system.

Modern gravimeters measure the gravitational field along the local vertical direction, which by definition is the direction of the gravitational field. A local density contrast because of UXO produces a contribution to the total field that is very small, e.g.,  $< 40$  ppb of the earth's main field, and only the vertical component ( $g_z$ ) of its contribution to the total field is discernible. The nominal gravitational acceleration ( $g_0$ ) the surface of the earth is  $9.8 \text{ m/s}^2$  ( $= 980$  Gals, where  $1 \text{ Gal} \equiv 1 \text{ cm/s}^2$ ). Gravimeters used for field surveying are relative instruments, i.e., they measure differences in the gravitational field. Thus, while the relative measurements above a buried UXO include the contributions of the UXO gravity field superimposed on the earth's gravity field, the measurements are usually referenced to an arbitrary base station value rather than to an absolute gravity benchmark (Butler 1980).

Most magnetometers in common use measure the magnitude of the total magnetic field in absolute terms. The magnetic field anomaly caused by a UXO (induced plus permanent components) will be smaller than the earth's main field but can be a much larger fraction of the main field than for gravity anomalies. Temporal variations in the earth's field are commonly removed using measurements from a base station recording magnetometer.

Relative to the physical properties of the UXO, the gravitational field depends on the mass (density and volume) and the distribution (orientation) of that mass relative to the measurement surface (Equations 1 and 2), while the magnetic field depends on the magnetization and its distribution through the UXO volume and the orientation of both relative to the surface of measurement (Equations 3 and 4). The magnetization of the UXO in turn is dependent on the inducing field, the magnetic susceptibility of the UXO material, and demagnetization effects of the geometry (Grant and West 1965).

For the special case where the density and magnetization of the UXO are uniform and constant, Equations 1 and 3 for the potentials simplify, respectively, to

$$U_P(\mathbf{r}) = -G \rho \iiint_R (1 / |\mathbf{r} - \mathbf{r}_0|) d^3r_0, \quad \text{and} \quad (6)$$

$$V_P(\mathbf{r}) = -\mathbf{M} \cdot \nabla \iiint_R (1 / |\mathbf{r} - \mathbf{r}_0|) d^3r_0. \quad (7)$$

When the magnetization is produced solely by the inducing earth's field (i.e., the UXO has no permanent magnetization),  $\mathbf{M}$  can be written  $\mathbf{M} = M \boldsymbol{\theta}$ , where  $\boldsymbol{\theta}$  is a unit vector in the direction of the earth's field  $\mathbf{H}_e = H_e \boldsymbol{\theta}$ , and Equation 7 becomes

$$V_P(\mathbf{r}) = -M (\partial / \partial \theta) \iiint_R (1 / |\mathbf{r} - \mathbf{r}_0|) d^3r_0 \quad (8)$$

and  $(\partial/\partial\theta)$  is the directional derivative in the direction of the earth's field. Demagnetization effects due to a spheroidal geometry (discussed later in this paper) are not considered in Equation 8. For this special case where  $M$  and  $\rho$  are constants, the identical volume integrals over the region of the UXO result in the relationship known as Poisson's relation (Grant and West 1965, Blakely 1995).

$$V_p(\mathbf{r}) = (M / G\rho) (\partial/\partial\theta) U_p(\mathbf{r}), \text{ or} \quad (9)$$

$$\mathbf{H}(\mathbf{r}) = (M / G\rho) (\partial/\partial\theta) \mathbf{g}(\mathbf{r}) \quad (10)$$

This relation allows a measured gravity field to be transformed into a pseudo-magnetic field and vice versa, if the density  $\rho$  and magnetic susceptibility  $k$  ( $M = k H_e$ , in the absence of the demagnetizing effects of the UXO geometry) are constant and the direction of the earth's field is known.

To use the above equations to compute a theoretical gravity or magnetic anomaly signature for a UXO, a model must be assumed for evaluation of the inverse distance-weighted volume integrals. The model is a geometric representation of the UXO. A first approximation to the geometry of UXO is a sphere with radius selected to give a mass equivalent to the actual UXO (Barrow, Khadr, and Nelson 1996). Another approximation that better represents the elongated geometry of UXO is a finite-length, right circular cylinder. An even better approximation to the geometry of UXO, which can still be handled analytically, is the prolate spheroid (McFee and Das 1990, Altshuler 1996, Butler et al. 1998).

## Model for UXO Gravity Response

The available gravity modeling approaches are not readily applicable to buried unexploded ordnance. Some of the approaches make inappropriate geometrical assumptions, such as two-dimensionality (2-D) of the sources, or require a complex parameterization of the source geometry, such as approximation of its surface by triangular planar facets or a complete discretization of the UXO source body. A realistic model for unexploded ordnance is a collection of homogeneous prolate spheroids. First, a reasonable approximation to the actual shape of the ordnance can be obtained by varying the spheroid parameters. Second, relatively few parameters are required to specify each spheroid: length, diameter, dip angle, and azimuth and density contrast. Third, a closed-form expression for the gravity field of a homogeneous spheroid (a special case of the general tri-axial ellipsoid) is known in terms of elementary functions (MacMillan 1958; Ramsey 1961). Thus, computing the gravity response of homogeneous spheroids should be straightforward. However, no software for modeling the gravity response of prolate spheroids is generally available. The prolate spheroid modeling capability for UXO was developed as an aid in evaluating the usefulness of gravity measurements in detecting unexploded ordnance. The geometry for the model development is shown in Figure 1.

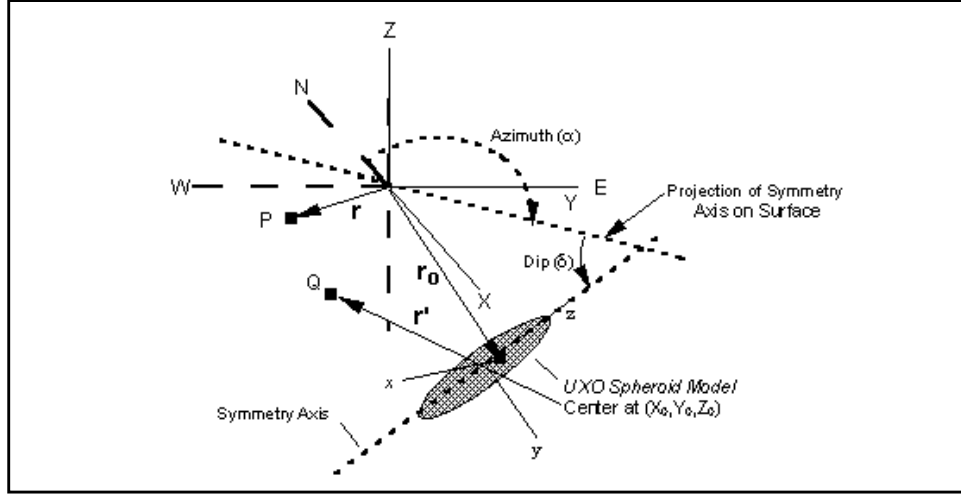


Figure 1. Geometry for UXO model development

Evaluating Equation 1 for exterior points to a homogeneous, tri-axial ellipsoid yields elliptic integrals of the first or second kind for the potential (MacMillan 1958, Arfken 1985). For the case of a spheroid, where two of the axes are equal, the elliptic integrals reduce to elementary integrals, which can be evaluated exactly. The anomalous gravitational potential at a point Q exterior to a spheroid is given by Equations 11 and 12, for the prolate ( $L > D$ ) and oblate ( $D > L$ ) cases respectively,

$$U_Q(r') = \pi G \rho D^2 L \left( 1 + \frac{x^2 + y^2 - 2z^2}{2(L^2 - D^2)} \right) \left( \frac{2}{\sqrt{L^2 - D^2}} \right) \sinh^{-1} \sqrt{\frac{L^2 - D^2}{D^2 + \kappa}} - \frac{\pi G \rho D^2 L \sqrt{L^2 + \kappa}}{L^2 - D^2} \left( \frac{x^2 + y^2}{D^2 + \kappa} \right) + \frac{\pi G \rho D^2 L}{L^2 - D^2} \left( \frac{2z^2}{\sqrt{L^2 + \kappa}} \right), L > D, \text{ and} \quad (11)$$

$$U_Q(r') = \pi G \rho D^2 L \left( 1 - \frac{x^2 + y^2 - 2z^2}{2(D^2 - L^2)} \right) \left( \frac{2}{\sqrt{D^2 - L^2}} \right) \sin^{-1} \sqrt{\frac{D^2 - L^2}{D^2 + \kappa}} + \frac{\pi G \rho D^2 L \sqrt{L^2 + \kappa}}{D^2 - L^2} \left( \frac{x^2 + y^2}{D^2 + \kappa} \right) - \frac{\pi G \rho D^2 L}{D^2 - L^2} \left( \frac{2z^2}{\sqrt{L^2 + \kappa}} \right), D > L, \quad (12)$$

where  $\rho$  is the UXO bulk density,  $D$  is the diameter,  $L$  is the length of the major axis,  $(x, y, z)$  are coordinates of Q are in the body-centered system ( $x$  and  $y$  along the minor axis and  $z$  along the major axis; Figure 1), and the elliptic distance function  $\kappa$  is given by

$$\frac{x^2 + y^2}{D^2 + \kappa} + \frac{z^2}{L^2 + \kappa} = 1 \quad (13)$$

The partial derivatives of  $U_Q$  with respect to  $x$ ,  $y$ , and  $z$  are the components of gravity in the body-centered coordinate system.

As noted in Equations 2 and 5, the gravity field components are given as the directional derivatives of the potential in Equations 11 and 12. The gravity measurements will be on the  $XY$ -plane (observation coordinate system), and the directional derivative of interest is  $\partial U/\partial Z$ . If the body-centered system is fixed with the  $x$ -axis horizontal, so that  $\partial x/\partial Z = 0$ , then the anomalous vertical component of gravity at point  $P$  in the observation coordinates is

$$\Delta g_{zP} = \frac{\partial U_P}{\partial Z} = \left( \frac{\partial U_P}{\partial y} \right) \left( \frac{\partial y}{\partial Z} \right) + \left( \frac{\partial U_P}{\partial z} \right) \left( \frac{\partial z}{\partial Z} \right) \quad (14)$$

where  $\partial U_P/\partial y$  and  $\partial U_P/\partial z$  are the required partial derivatives of Equations 11 or 12.

The observation coordinate system is connected to the body-centered system by a translation and rotation

$$\begin{aligned} (\mathbf{X}, \mathbf{Y}, \mathbf{Z}) &= (\mathbf{X}_0, \mathbf{Y}_0, \mathbf{Z}_0) + \mathbf{A} \cdot (\mathbf{x}, \mathbf{y}, \mathbf{z}), \text{ or inversely} & (15) \\ (\mathbf{x}, \mathbf{y}, \mathbf{z}) &= \mathbf{A}^{-1} \cdot [(\mathbf{X}, \mathbf{Y}, \mathbf{Z}) - (\mathbf{X}_0, \mathbf{Y}_0, \mathbf{Z}_0)], \end{aligned}$$

where  $\mathbf{A}$  is the Euler rotation tensor (Arfken 1985).

For a buried ordnance item model, the depth is to the geometric center. The inclination or dip ( $\delta$ ) of the spheroid is relative to the  $XY$  plane, and thus a dip of 90 deg is vertical. Azimuth ( $\alpha$ ) of the spheroid is defined as the angle between a vertical plane through the long axis of the spheroid and north, with clockwise angles positive (Figure 1) and an azimuths of 0 deg and 180 deg are north-south.

Using the inverse coordinate transformation relation from Equation 15, the gravity field in observation coordinates becomes

$$\Delta g_z(X, Y) = - \left( \frac{\partial U}{\partial y} \right) \cos \delta + \left( \frac{\partial U}{\partial z} \right) \sin \delta \quad (16)$$

where the expressions for the partial derivatives are evaluated in observation coordinates. The prolate spheroid gravity modeling program computes the vertical component of the anomalous gravity field on the  $XY$ -plane over a specified area with specified grid spacing. The case  $L = D$  (a sphere) is treated separately in the program using the familiar analytical solution for a sphere; however, Equations 11 and 12 are well-behaved as  $L \rightarrow D$  (but  $L \neq D$ ), approaching the sphere solution.

For comparison of the calculated gravity anomaly with measured gravity data, the measured data must be related to a local gravity base station and corrected for all known sources of spatial and temporal variation to give anomaly data (Chapter 4, herein, and Butler 1980). The resulting anomaly data may still contain superimposed larger spatial wavelength gravity variations (local regional

gravity field). Removing the larger spatial wavelength gravity component results in an anomaly, termed the residual anomaly, which can then be compared to computed anomalies.

When the prolate spheroid with bulk density  $\rho$  is surrounded by earth material with density  $\rho_e$ , it is the density contrast  $\Delta\rho = \rho - \rho_e$  that is responsible for the gravity anomaly and which must be used in the spheroid modeling program. The excess mass  $\Delta\text{Mass}$  ( $= \Delta\rho \cdot V$ , where  $V$  is the volume) associated with the density contrast is estimated by application of Gauss' Law to vertical gravity component measurements on the observation plane (XY-plane) (Blakely 1995, Butler 1980).

$$\begin{aligned} \Delta\text{Mass} &= \left(\frac{1}{2\pi G}\right) \int_S \Delta g_z dS = \left(\frac{1}{2\pi G}\right) \int_{-\infty}^{\infty} \Delta g_z dXdY \\ &\approx \left(\frac{1}{2\pi G}\right) \sum_i \Delta g_{zi} \Delta X \Delta Y \end{aligned} \quad (17)$$

where the second equation above assumes values *calculated or measured* on a grid of dimensions  $\Delta X \Delta Y$ , the index 'i' refers to the  $i^{\text{th}}$  grid cell, and the summation clearly must be carried out to regions of the XY-plane where  $\Delta g_{zi} \neq 0$ . If the spheroid bulk density and density contrast are known or can be estimated, the total mass of the spheroid is given or estimated as

$$\text{Mass} = \left(\frac{\rho}{\Delta\rho}\right) \Delta\text{Mass} \quad (18)$$

## UXO Gravity Modeling Program

The spheroid model for UXO was originally developed in FORTRAN and subsequently converted to C++. The C++ program has a Windows graphical user interface (GUI) to facilitate parameter input and execution. Program input consists of the following:

- a. Specification of calculation grid (size limits and intervals):

Xmin, Xmax, delta-X  
Ymin, Ymax, delta-Y

- b. Specification of geometric center of spheroid:

Xo, Yo, Zo

- c. Length, diameter, and density contrast of spheroid:

Length (L), Diameter (D), Density ( $\Delta\rho$ )

*d.* Orientation of spheroid:

Dip ( $\delta$ ), Azimuth ( $\alpha$ )

All distance parameters are in meters (m), the density contrast is in  $\text{g/cm}^3$ , and dip and azimuth angles are in degrees relative to horizontal and north, respectively. An optional input data file can be specified or alternatively input via the GUI data entry form. The program writes the computed gravity anomaly values as an ASCII file to a specified output file. The output file is then read by a database program to perform mass calculations (Equations 17 and 18) or by a general-purpose plotting program to produce contour or profile plots of the calculation results. Gravity anomaly values are in microgal ( $\mu\text{Gal}$ ). The microgal is a convenient unit for gravity anomalies produced by UXO (Chapters 3 and 4).

# 3 UXO Prolate Spheroid Model: Gravity Anomaly Calculations

## Bulk Density of Representative Ordnance Items

While the total field magnetic anomaly signature is relatively independent of the magnetic permeability as long as  $\mu_r > 150$  (where  $\mu_r$  is the relative magnetic permeability), the gravity signature is directly dependent on the bulk density contrast. The bulk density of ordnance items varies from  $\sim 3 \text{ g/cm}^3$  to  $> 6 \text{ g/cm}^3$ . For a typical soil density of  $2 \text{ g/cm}^3$ , the density contrast will vary from  $\sim 1.2 \text{ g/cm}^3$  to  $> 4 \text{ g/cm}^3$ . Parameters for selected ordnance items for use in signature modeling with GRAVMOD are given in Table 1.

<b>Table 1 Average Parameter Sets for Ordnance Item Models</b>				
<b>Ordnance Item</b>	<b>Length (m)</b>	<b>Diameter (m)</b>	<b>Mass (kg)</b>	<b>Bulk Density (g/cm<sup>3</sup>)</b>
105-mm Projectile	0.48	0.105	15.3	5.4
155-mm Projectile	0.70	0.155	45.2	5.2
175-mm Projectile	0.87	0.175	66.8	4.8
8-in. Projectile	0.86	0.203	98.4	5.4
12-in. Projectile	1.21	0.304	393.6	6.5
14-in. Projectile	1.48	0.356	638.9	6.6
16-in. Projectile	1.69	0.406	1031.5	7.0
500-lb Bomb	1.59	0.266	236.7	4.1
750-lb Bomb	1.25	0.406	337	3.2
1,000-lb Bomb	1.84	0.339	453.7	4.2
2,000-lb Bomb	2.50	0.457	907	3.4

The length, diameter, mass, and bulk density in Table 1 represent an average of up to five specific cases for each ordnance item entry.

## Investigation of Gravity Anomalies of Prolate Spheroid Models of UXO

The features of the gravity anomaly for a prolate spheroid model are illustrated in Figure 2, for a 14-in. projectile model. For a horizontal spheroid model, the gravity anomaly is symmetric about two horizontal axes (Figure 2a). As the dip increases from zero, the anomaly is symmetric only about the projection of the major axis of the spheroid on the surface (Figure 2a and 2b). Unlike the total field magnetic anomaly, which is induced by the earth's field, the gravity anomaly field for a prolate spheroid model of UXO follows (i.e., does not lag) the azimuth of the spheroid. The gravity anomaly is rotationally symmetric about a vertical axis as the spheroid azimuth varies (Figures 2b and 2c). Doubling the depth of the spheroid from 0.3 m to 0.6 m results in a peak field decrease from  $\sim 22$  to  $\sim 7$   $\mu\text{Gal}$  (Figures 2c and 2d), along with the expected increase in anomaly width (spatial wavelength). The anomalies for all cases in Figure 2 are detectable with a well-executed microgravity survey. However, a 14-in. projectile is quite large (comparable to a 1,000-lb bomb in size, but with greater density).

Compare the anomalies in Figure 2 with the cases in Figure 3 for a 155-mm projectile at depths of 0.1 and 0.2 m, where the peak magnitude decreases from  $\sim 8$  to  $\sim 3$   $\mu\text{Gal}$ , respectively, as the depth is doubled. A 155-mm projectile at a depth of 0.2 m could only be detected with an extremely carefully executed microgravity survey. Applying Equations 17 and 18 to the 0.1-m depth anomaly for the 155-mm model results in a computed excess mass of 27.5-kg, which corresponds to a total mass of 44.7 kg. The actual mass of the 155-m projectile used for the model is 43 kg, i.e., the calculated mass is approximately 4 percent greater in this case. For the 0.2-m depth anomaly, the computed total mass is 42.2 or approximately 2 percent less than the actual model mass. Much of the differences in computed mass and actual model mass can be attributed to rounding in the anomaly calculations and in the spreadsheet calculations. However, as the depth increases for a given ordnance item model and for a fixed calculation area size, the calculated mass will be increasingly *less* than the model mass due to more of the total anomaly located outside the calculation area (i.e.,  $\Delta g_{zi} \Rightarrow 0$  within the calculation area).

All of the gravity anomalies in Figures 2 and 3 indicate that the causative source (in this case, the model) is elongated, i.e., compared to the perfectly symmetrical anomaly produced by a spherical source model. For all compact three-dimensional models regardless of their geometrical complexity, a source depth exists such that the gravity anomaly is indistinguishable from the anomaly due to a spherical source. Figures 4 through 6 investigate the nature of prolate spheroid model gravity anomalies relative to spherical model gravity anomalies. In Figure 4, the maximum gravity anomaly value for a 155-mm projectile model is compared to an equivalent volume spherical model as a function of depth. For depths greater than 0.5 m, the maximum gravity anomaly value caused by a 155-mm projectile prolate spheroid model is identical to an equivalent volume spherical model.

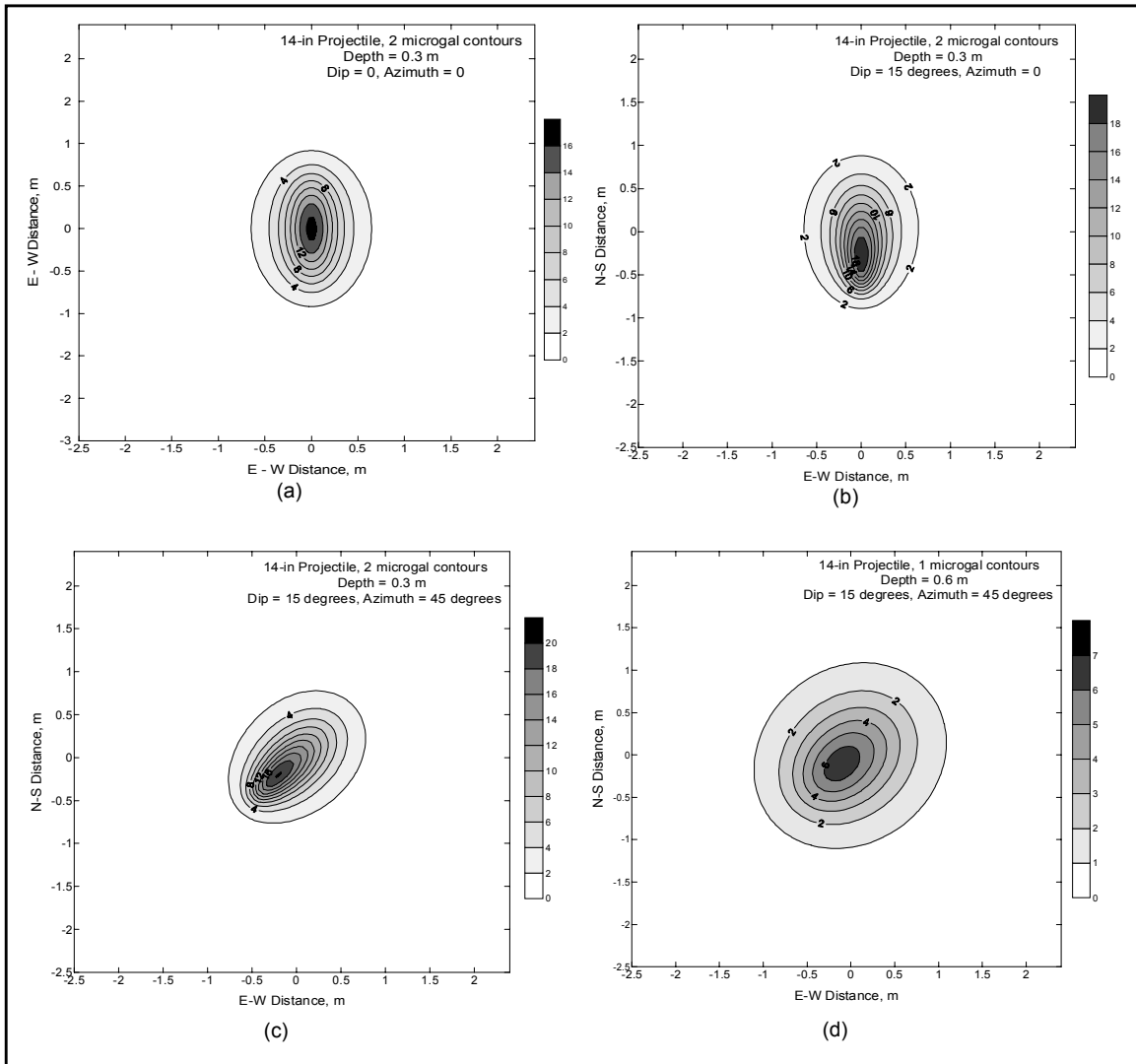


Figure 2. Gravity anomalies above a 14-in. projectile spheroid model for the cases: (a) depth = 0.3 m, dip = 0, azimuth = 0; (b) depth = 0.3 m, dip = 15 deg, azimuth = 0; (c) depth = 0.3 m, dip = 15 deg, azimuth = 45 deg; (d) depth = 0.6 m, dip = 15 deg, azimuth = 45 deg

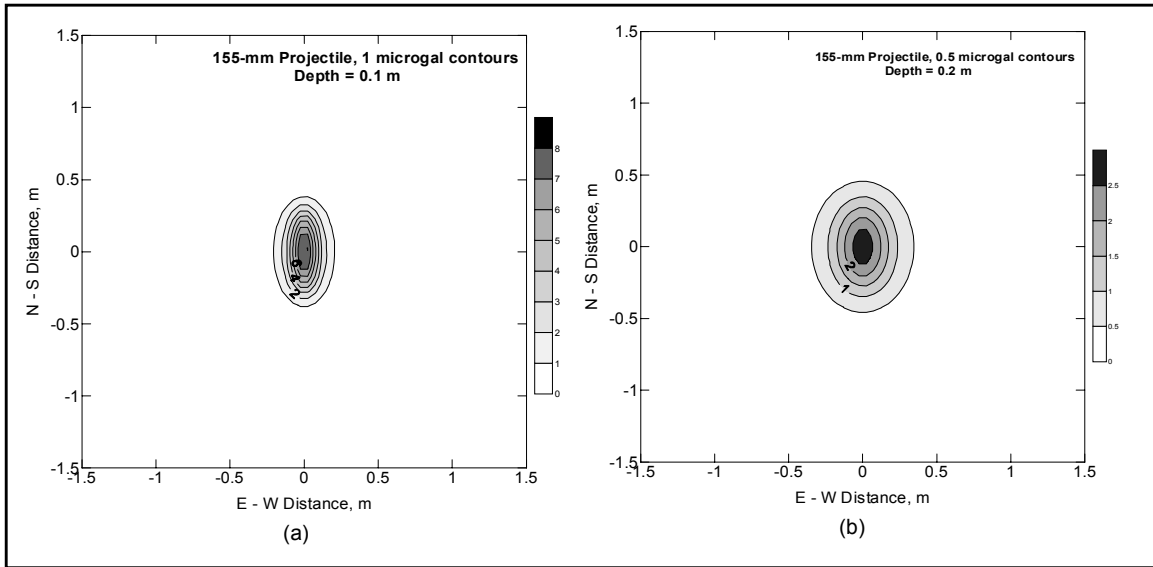


Figure 3. Gravity anomalies above a 155-mm projectile spheroid model, with dip = 0 and azimuth = 0, for the cases: (a) depth = 0.1 m; (b) depth = 0.2 m

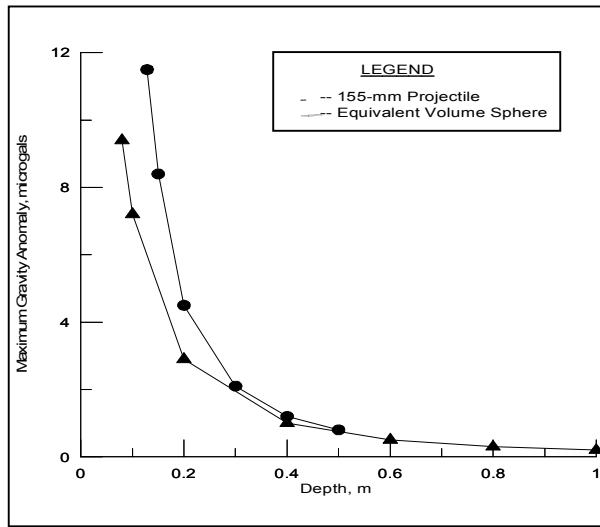


Figure 4. Comparison of maximum gravity anomaly for a 155-mm prolate spheroid and an equivalent volume sphere models

The prolate spheroid model gravity anomalies are distinguished by different “spatial wavelengths” in the orthogonal directions along the major and minor axes. A “spatial wavelength” for a gravity anomaly is defined as the distance along a given profile direction between the half-maximum anomaly points ( $\lambda_{1/2}$ ). Gravity profiles along the major and minor axis directions for the two cases in Figure 3 are shown in Figure 5, where the horizontal plot axes are equal and the vertical plot axes are proportional, to facilitate comparison of the spatial wavelengths. The maximum and half-maximum values are indicated in Figure 5, and the wavelength for the major axis is defined in Figure 5b. Both the major and minor axis-direction spatial wavelengths increase as a function of depth.

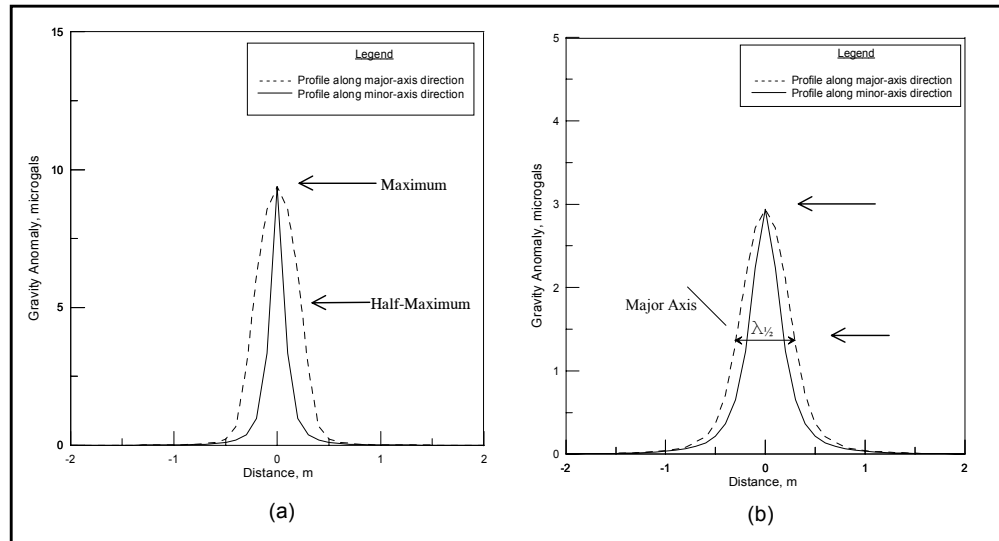


Figure 5. Gravity profiles along the major- and minor-axis directions for the cases in Figure 3: (a) 155-mm projectile model, depth = 0.1 m; (b) 155-mm projectile model, depth = 0.2 m

For a spherical model, the gravity anomaly is circularly symmetrical and the spatial wavelength is related to the depth ( $Z_0$ ) by the expression  $\lambda_{1/2} = 1.53 Z_0$ . As noted above, at a sufficiently large depth, the gravity anomaly of a spheroid model will become indistinguishable from the gravity anomaly of a spherical model. The three spatial wavelengths, the major and minor spheroid wavelengths and the spherical wavelength, are plotted as a function of depth in Figure 6 for a 1,000-lb bomb spheroid model. Plots of the three wavelength measures converge and for depths greater than approximately 2 m are equal. The nominal and maximum-likely detection depths (see following section and Chapter 4, this report) for the prolate spheroid are indicated. Since the major- and minor-axis spatial wavelengths are clearly distinct to depths greater than the maximum-likely detection depth, the elongated nature of the source body will be evident.

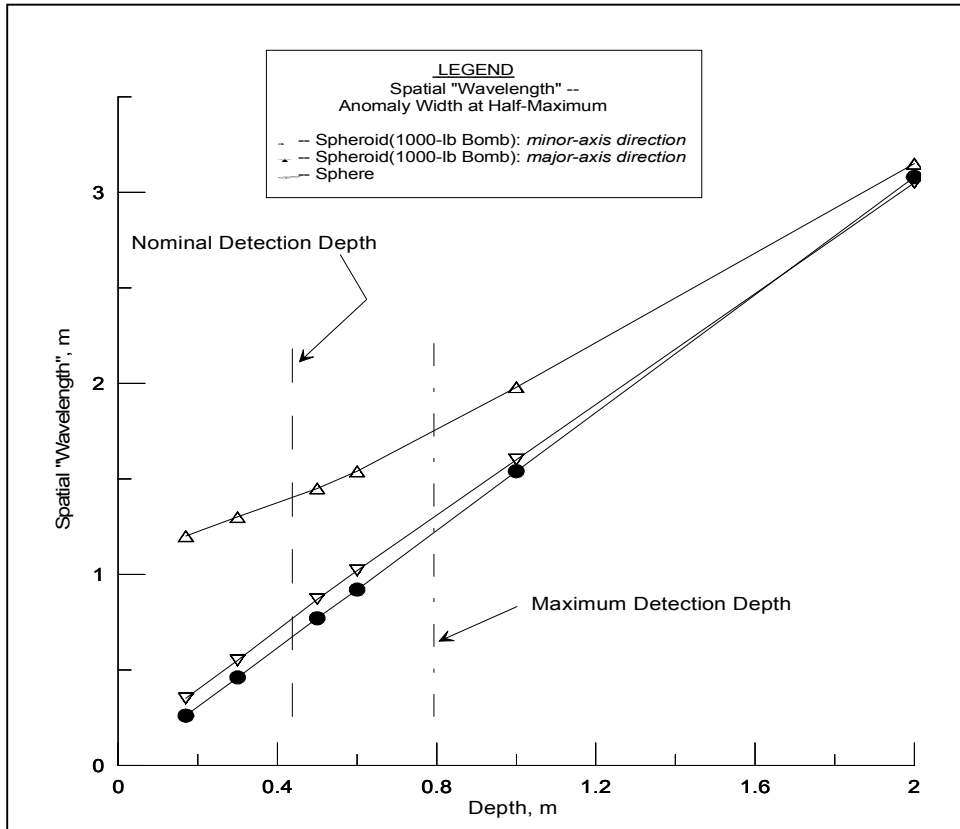


Figure 6. Spatial wavelengths for 1,000-lb bomb spheroid model (along major and minor axes) and for a spherical model

## Gravity Anomalies of Representative Ordnance Items

Gravity anomaly calculations similar to those shown in Figures 2 and 3 were performed for all the representative ordnance items in Table 1 as a function of depth. For these calculations, the spheroid models of the ordnance items were horizontal. The results of the calculations are summarized in Figure 7, where the maximum gravity anomaly values for all ordnance items are plotted as a function of depth. The smallest or shallowest depth for each ordnance item is for the upper surface of the item at the ground surface (i.e., the depth is equal to the radius of the item). The maximum gravity anomaly produced by any of the ordnance items is 40  $\mu\text{Gal}$ .

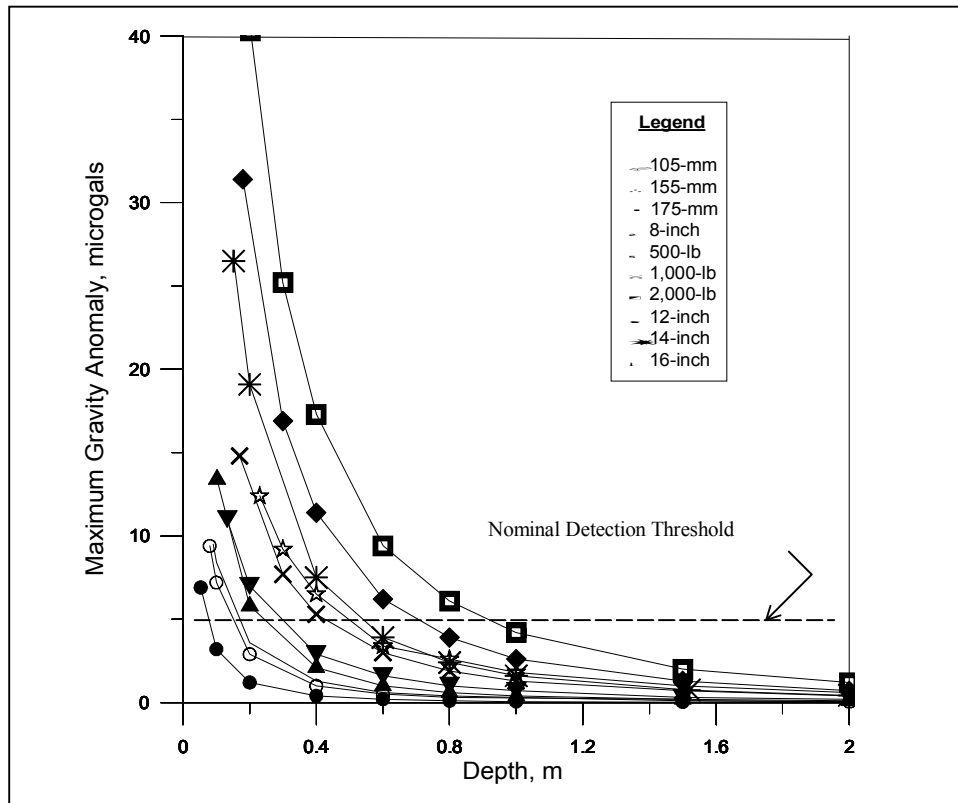


Figure 7. Maximum gravity anomaly values for representative ordnance items oriented horizontally

## Detectability Considerations

Three factors determine whether a gravity anomaly will be detectable and recognizable: (1) the magnitude of the anomaly, (2) the spatial wavelength of the anomaly relative to the measurement or calculation spacing (Nyquist spatial sampling considerations), (3) anomaly signal to site-specific noise considerations. For manual microgravimeters (such as the LaCoste and Romberg Model D, with electronic levels and readout options), Butler (1980) establishes a basic measurement accuracy of 2 to 3  $\mu\text{Gal}$  for a single measurement and 5  $\mu\text{Gal}$  for a relative gravity determination (i.e., relative to a base station measurement). This measurement accuracy is for a set of very carefully executed measurements, in an area without significant topographic variation within the survey area and includes both measurement and correction errors (Chapter 4).

Typical microgravity survey areas are in the range of 500 to 10,000  $\text{m}^2$ , with measurement spacing of 2 to 10 m. For these typical microgravity surveys, a rule of thumb is that anomalies with magnitude  $\geq 10 \mu\text{Gal}$  (i.e., two times the basic measurement accuracy) are routinely detectable. For the small area microgravity surveys proposed for UXO, the survey areas could be in the range 10 to 50  $\text{m}^2$  with measurement spacing of 0.25 to 0.5 m. The measurement accuracy and

anomaly detectability should improve for these smaller area surveys, and a *nominal detection threshold of 5  $\mu$ Gal* is reasonable. The basic *reading* accuracy and practical sensitivity of the manual microgravimeters is approximately 1  $\mu$ Gal. However, as discussed by Ander et al. (1999), the thermodynamic noise limit of the gravimeter sensor is 0.012  $\mu$ Gal, and there is no fundamental limitation to improving measurement accuracy to 0.1  $\mu$ Gal or better. This improvement in measurement accuracy is approached with new digital gravimeters that use force feedback nulling, real-time off-level and earth tide corrections, ensemble averaging, and digital recording. For the new gravimeters, a *minimum detection threshold of 2  $\mu$ Gal* is feasible.

Associated with the 5- $\mu$ Gal nominal detection and the 2- $\mu$ Gal minimum detection thresholds are detection depths, the nominal and the maximum, respectively, for each ordnance item. These two detection depths are indicated in Figure 6 for a 1,000-lb bomb. The 5- $\mu$ Gal detection threshold is shown in Figure 7. Nominal and maximum detection depths for all ordnance items in Figure 7 are summarized in Table 2.

<b>Table 2 Nominal and Maximum Gravity Anomaly Detection Depths for Representative Ordnance Items (from Figure 7)</b>		
<b>Ordnance Item</b>	<b>Nominal Detection Depth, m</b>	<b>Maximum Detection Depth, m</b>
105-mm Projectile	.09	.17
155-mm Projectile	.16	.30
175-mm Projectile	.18	.35
8-inch Projectile	.25	.40
500-lb Bomb	.31	.54
1,000-lb Bomb	.43	.78
2,000-lb Bomb	.50	.90
12 inch Projectile	.55	.92
14-inch Projectile	.72	1.20
16-inch Projectile	.93	1.50

While the definition of “spatial wavelength” used in this report is only an approximate characterization of the spatial spectra of the gravity anomalies, adequate definition of the anomaly is achieved for measurement spacing  $\Delta x \sim \lambda_{1/2} / 2$  (Butler 1980; Blakely 1995). Considering the results presented in Figures 2, 3, 5, and 6 and other ordnance item gravity anomalies calculated during this study, measurement spacing in the range of 0.25 to 0.75 m is required (nominal spacing of 0.5 m). Surveys with measurement spacing this small, in the experience of the author, will be the highest spatial resolution microgravity surveys ever conducted.

Once an anomaly exceeds the minimum and/or nominal detection thresholds defined above, the problem becomes a detection and a recognition issue relative to the site-specific background. Like the considerations of backgrounds for TFM and TDEM surveys, the background for microgravity surveys consists of geologic and cultural components. For shallow, localized density anomalies like a buried UXO, the gravity anomaly will be compact, closed anomaly contours. Only other

shallow, dense, localized subsurface features will produce anomalies with magnitudes and spatial wavelengths comparable to UXO. For the geologic background component, there is no experience with the small survey areas and measurements spacing referenced above for UXO detection surveys. For typical microgravity survey areas and measurement spacing, experience has shown that most site-specific anomalies resulting from deeper geologic features and soil and rock type changes will have longer wavelengths than UXO anomalies and, if closed, will be easily separated from UXO anomalies. Anomalies caused by very shallow geologic heterogeneity will be low magnitude and tend to be randomly distributed. The other types of geologic features that could produce closed anomaly features with magnitudes comparable to UXO anomalies are boulders in the shallow subsurface and cavities and other features associated with karst features. Fortunately, anomalies caused by cavities, sinkholes, and clay pockets in the top of rock will be negative, i.e., corresponding to a negative density contrast relative to surrounding soil and rock. Thus, only boulders and features like limestone pinnacles at the top of rock can produce short, spatial-wavelength-positive geologic anomalies, although the *density contrast* of these features will be less than for the ordnance items listed in Table 1, nominally  $0.5 \text{ g/cm}^3$  for limestone pinnacles and from  $0.5$  to  $1.0 \text{ g/cm}^3$  for boulders.

The only type of cultural features which could be problematic for UXO gravity anomaly recognition are *compact* metallic objects, e.g., an engine block, electric motor, piece of structural steel, etc., with *bulk density* comparable to UXO. Relatively flat metal plates, while having bulk density greater than UXO, will produce distinctively different gravity anomalies. For example, a 1-m by 1-m by 1-cm-thick steel plate will have mass comparable to a 175-mm projectile and, if oriented horizontally just below the surface ( $\leq 10$  cm depth), will produce a  $2\text{-}\mu\text{Gal}$  anomaly above its center, but it will have a gravity anomaly that is nearly symmetric about a vertical axis. The same steel plate oriented vertically (and  $\leq 10$  cm depth) will produce an anomaly  $< 1 \mu\text{Gal}$  and have an extremely small spatial wavelength transverse to the plate.

# 4 Relevant Microgravimetry Surveys for UXO Detection Considerations

---

## Background

The nominal gravitational acceleration on the surface of the earth is  $9.8 \text{ m/s}^2$  ( $= 980 \text{ Gal}$ , where  $1 \text{ Gal} \equiv 1 \text{ cm/s}^2$ ). Microgravimetry refers to specialized high-accuracy and generally high-resolution gravity surveying, where the objective is to measure gravity to an accuracy of  $\sim 1 \text{ } \mu\text{Gal}$  or  $10^{-9}$  times the nominal earth acceleration (Butler 1980). After correction of the measurements for all known sources of variation in the earth's gravitational field, the results of a microgravity survey are anomalies caused by small, shallow density contrasts. The density contrasts can be localized, buried cultural, or natural geologic features. Density contrasts can also be caused by changes in subsurface conditions, such as variation in depth to water table or top of rock. The necessary condition for *existence* of a gravity anomaly is a lateral (localized) contrast in density, and the magnitude of the gravity anomaly is a function of the density contrast and the geometry, size, and depth of the feature. The basic or theoretical conditions for detection of a gravity anomaly are that the anomaly magnitude exceeds the *corrected* measurement accuracy and that the measurement spacing be sufficiently small to resolve the anomaly spatial wavelength. However, practical anomaly detection will only occur when the magnitude and spatial wavelength of an anomaly of interest can be distinguished relative to the site-specific background gravity variations.

Traditional applications of gravity surveys are for global-scale structure studies, regional geologic mapping, petroleum exploration, and mining applications. Microgravity surveys are generally local-scale surveys with objectives such as detecting and mapping cavities and tunnels (Butler 1984), low-density zones in structural foundations (Yule et al. 1998), landfill characterization (Hinze, Roberts, and Leap 1990), and special applications (Sjostrom and Butler 1996; Butler, Sjostrom, and Llopis 1997). Detection of UXO by microgravity surveys is a very challenging special application of microgravimetry.

## Microgravity Survey and Measurement Procedures

Typical microgravity survey areas and measurement spacing as well as the special requirements for UXO applications are discussed in the previous sections. This section will summarize the procedures of conducting a microgravity survey and necessary data corrections. Detailed microgravity survey and data correction procedures are found in reports by Butler (1980), ASTM (2000) and Burger (1992). Once the survey area is selected, a measurement grid or set of profile lines is established. Data correction requirements dictate horizontal location accuracy of 1 m or better (clearly for UXO surveys, ~ 10 cm is required) and vertical accuracy of 0.3 cm, in order to keep correction errors due to location less than 1  $\mu\text{Gal}$ . Commonly a base station is selected at one corner or within the survey area. The base station serves as a reference elevation and latitude for the survey and often also for the baseline gravity value, i.e., all gravity values in the survey are relative to the base station reading. The survey procedure seeks to minimize random and systematic error sources and requires patience and consistency for the measurements. For typical microgravity surveys, each measurement typically requires 4 to 5 min, including transport over distances of 2 to 6 m and meter leveling. For transport over distances of 0.25 to 0.75 m, the measurement time may decrease to 2 to 4 min, but likely not much less. The gravity measurements are acquired in loops through the grid of 6 to 10 stations prior to returning to the base station in less than 1 hr and preferably 30 to 45 min. The reasons for this survey procedure and the details of the actual measurement process are discussed in Butler (1980).

The objective of correcting gravity data is to account for all known sources of gravity variation. Gravity varies with elevation (i.e., elevation differences within the survey area), latitude, and time, due to the effects of topographic (terrain) features and manmade structures within and adjacent to the survey area, and due to the gravity effects of geologic features below the depth of interest of the surveys (the local regional field). The elevation correction consists of two parts: the free-air correction that accounts for varying distances from the center of the earth of the measurement points; the Bouguer correction that accounts for varying thickness of surficial-density material beneath the measurement point. The free-air and Bouguer corrections are added or subtracted depending on the elevation of the measurement points relative to a base station value or other reference gravity value. Likewise the time correction consists of two parts: a correction for the solid earth tide gravity variation; a correction for instrument drift and tares. A terrain correction accounts for the gravity effect of topographic features (hills, valleys, manmade structures); this correction is always added to measured gravity. The terrain correction for large topographic features outside the survey area is sometimes included as part of the local regional field. Gravity anomalies are named depending on the number of corrections applied to the measurements:

- a.* Free-air anomaly—the free-air and time corrections are applied.
- b.* Simple Bouguer anomaly—in addition to *a.* includes the Bouguer correction.

- c. Complete Bouguer anomaly—in addition to a. and b. includes the terrain correction.
- d. Residual anomaly—a local regional gravity field is subtracted from c.

The regional-residual separation process (item d above) is often considered an interpretation step, since the local regional field must be determined from the survey data or from auxiliary data (Butler 1980; Butler et al. 1982). Once determined, the residual anomaly is due to gravity sources within the depth of interest; generally defined by the size of the survey area and/or the procedure used to determine the local regional field.

## Microgravity Surveys—Case Histories

Two mini-case histories illustrate gravity detection and resolution concepts and geologic and cultural gravity backgrounds. A case history frequently cited as defining the possibilities of microgravimetry is documented by Butler (1980), Butler (1984), Burger (1992), ASTM (2000), and National Research Council (2000). The survey, which was conducted over a cavity test site in Florida, consisted of 420 gravity stations on a 3-m (10-ft) grid and was performed with a LaCoste and Romberg Model D manual gravimeter with standard level bubbles and electronic readout. A residual gravity anomaly profile from this case history is shown in Figure 8, along with a geologic cross section derived from shallow borings. A planar local regional field (i.e., a long wavelength background) has been subtracted to yield the residual anomaly. The anomaly profile illustrates two types of features: (1) detection of known air-filled cavities below the surface of limestone “bedrock,” and (2) detection of undulations (limestone pinnacles and clay pockets) in the top of rock. *Importantly, the gravity anomaly profile confirms detection of anomalies in the 5 to 10  $\mu$ Gal range that are correlated to known (geologic) features.* The localized anomalies in Figure 8 have spatial wavelengths of 3 to 6 m. Such anomalies as part of the geologic background could complicate detection and recognition of UXO gravity anomalies, but are still larger than UXO anomaly spatial wavelengths.

A second microgravity survey example is presented in Figures 9 and 10. This survey was conducted at an abandoned UST site with a Scintrex CG-3M digital gravimeter. The gravity anomaly map over three UST’s is shown in Figure 9, where the center lines of the UST’s are shown. The gravity anomaly is the superposition of the anomalies produced by all the UST’s, and the individual UST’s are not resolved in the data. The site for this survey is complicated by numerous, large-surface concrete structures and terrain features that affect the gravity data (i.e., gravity data are not corrected for the presence of the surface features). A north-south profile line, designated the 40E profile, is indicated in Figure 9, and observed and calculated gravity profiles along this line are shown in Figure 10. The calculated gravity profile is for a 2-D model of the known subsurface conditions along the line. The profile line crosses the two large UST’s, 8-ft diameter, 30.8-ft length, and separated by 2-ft (2.43-m diameter, 9.39-m length, 0.61-m separation) transverse to their center lines. Depth to the top of the UST’s is 3 ft (~ 1 m). The 2-D approximation is valid for this case

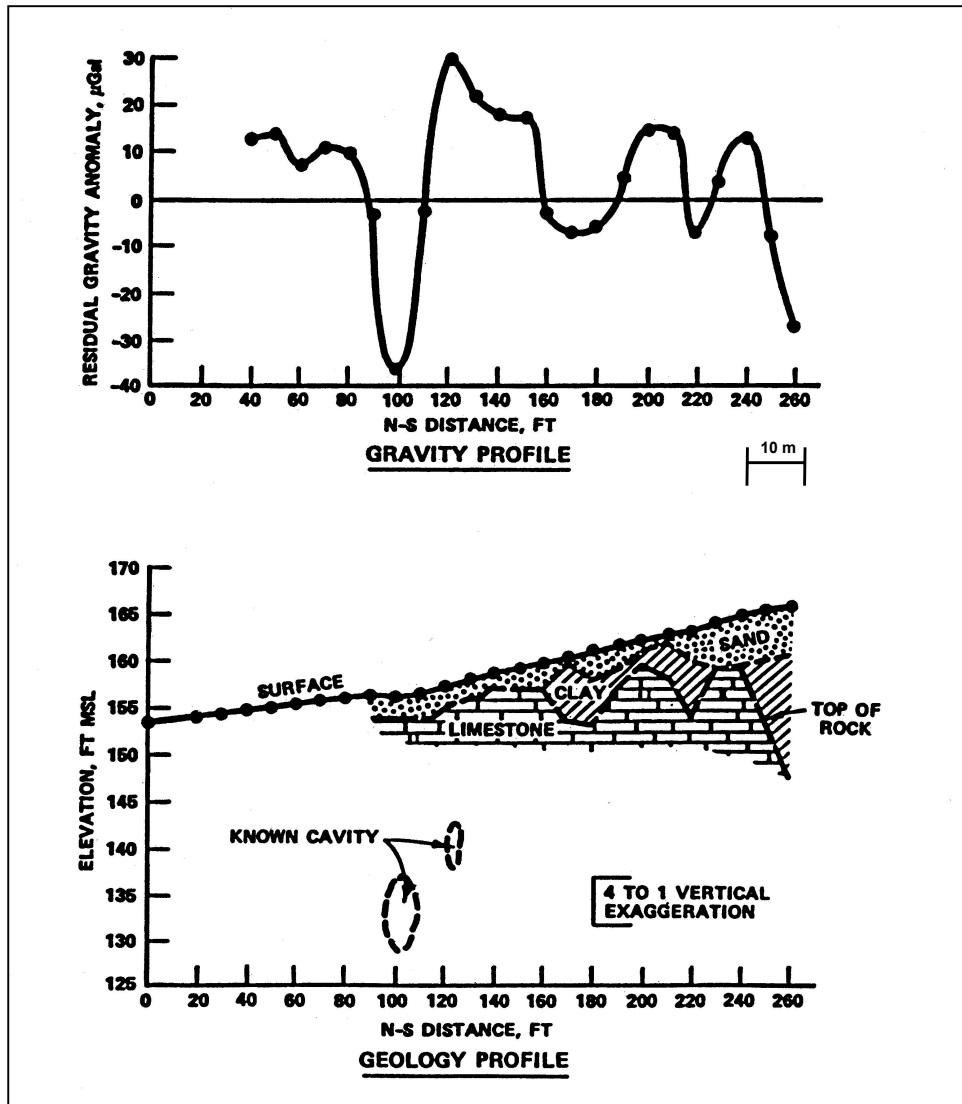


Figure 8. Residual gravity anomaly profile and associated geologic cross-section

(Butler 1980). Density contrasts indicated in the gravity model are relative to the surrounding soil. The model fit to the observed data is good except for the southern end, where the gravity terrain effects of the surface features are not corrected. Since terrain corrections are always added, the relation of the observed to model plots for the south end are consistent. An anomaly of this type (Figure 9), i.e., closed but with large spatial wavelength, will not pose difficulty for recognition of gravity anomalies of UXO. The centers of the two UST's are spaced slightly more than the distance required for theoretical resolution (Butler 1980), as noted in the model gravity profile. The measurements were too coarsely spaced (10 ft or 3 m) in this survey to achieve practical resolution.

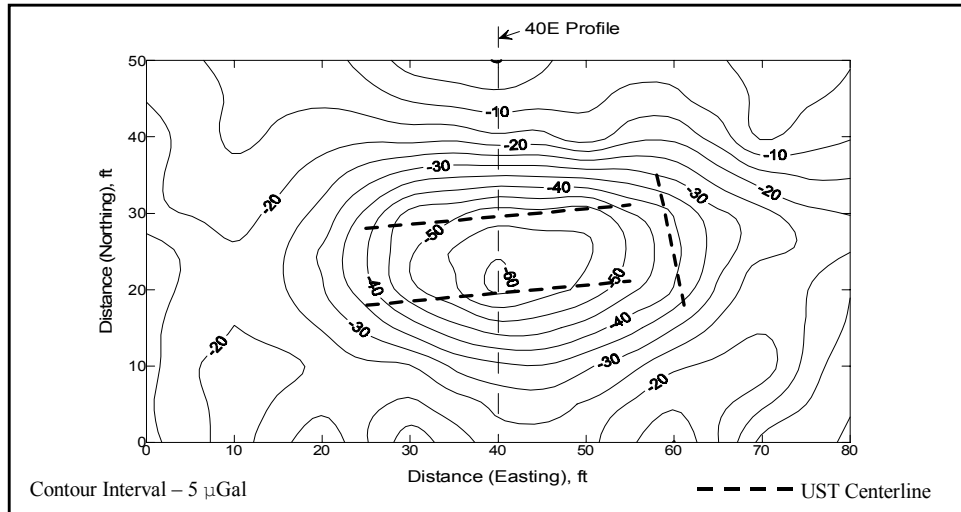


Figure 9. Gravity anomaly above three USTs

## Microgravity Survey over an Ordnance Item

Two microgravity investigations were planned as part of assessing the potential for UXO detection and discrimination. The first investigation was over an abandoned 100-gal buried fuel tank using a Scintrex CG-3M gravimeter. A 3- $\times$  3-m survey area with 0.5-m station spacing and two 5-m long orthogonal profile lines were established, centered on the tank. Surveys were conducted over the tank along the two profile lines, when the tank was empty (before) and filled (after) with water. The objective was to discriminate between two “false alarm” anomalous mass conditions. *The before and after surveys did indicate a gravity difference although there is considerable scatter in the corrected gravity profile data: before, - 15  $\mu$ Gal; after, + 9  $\mu$ Gal.* Thus, the before-after difference was 24  $\mu$ Gal, which is a factor of 8 to 10 larger than predicted theoretically. There were a number of factors that make the results suspect: erratic gravimeter performance with high drift rates; high standard deviations on the recorded measurements; extremely hot and humid operating conditions; occurrence of large earthquake during the surveys (magnitude 6.9 in Mexico); a compressor in an adjacent building turned on and off periodically during the surveys; and water spilled on the ground during filling the tank, increasing the shallow soil density by an unknown amount. For these reasons, the results of this first investigation will not be discussed in detail. A revisit of this investigation is planned for a future date.

The second investigation was a survey over an inert 155-mm projectile. A plan and cross-sectional view of the survey area and photograph of the projectile burial are shown in Figure 11. The 155-mm projectile, with 0.637-m length, 0.155-m diameter, and 45.25-kg mass, was buried in a horizontal orientation at 0.09-m depth to the top. For reference, the location and elevation of the site are as follows:

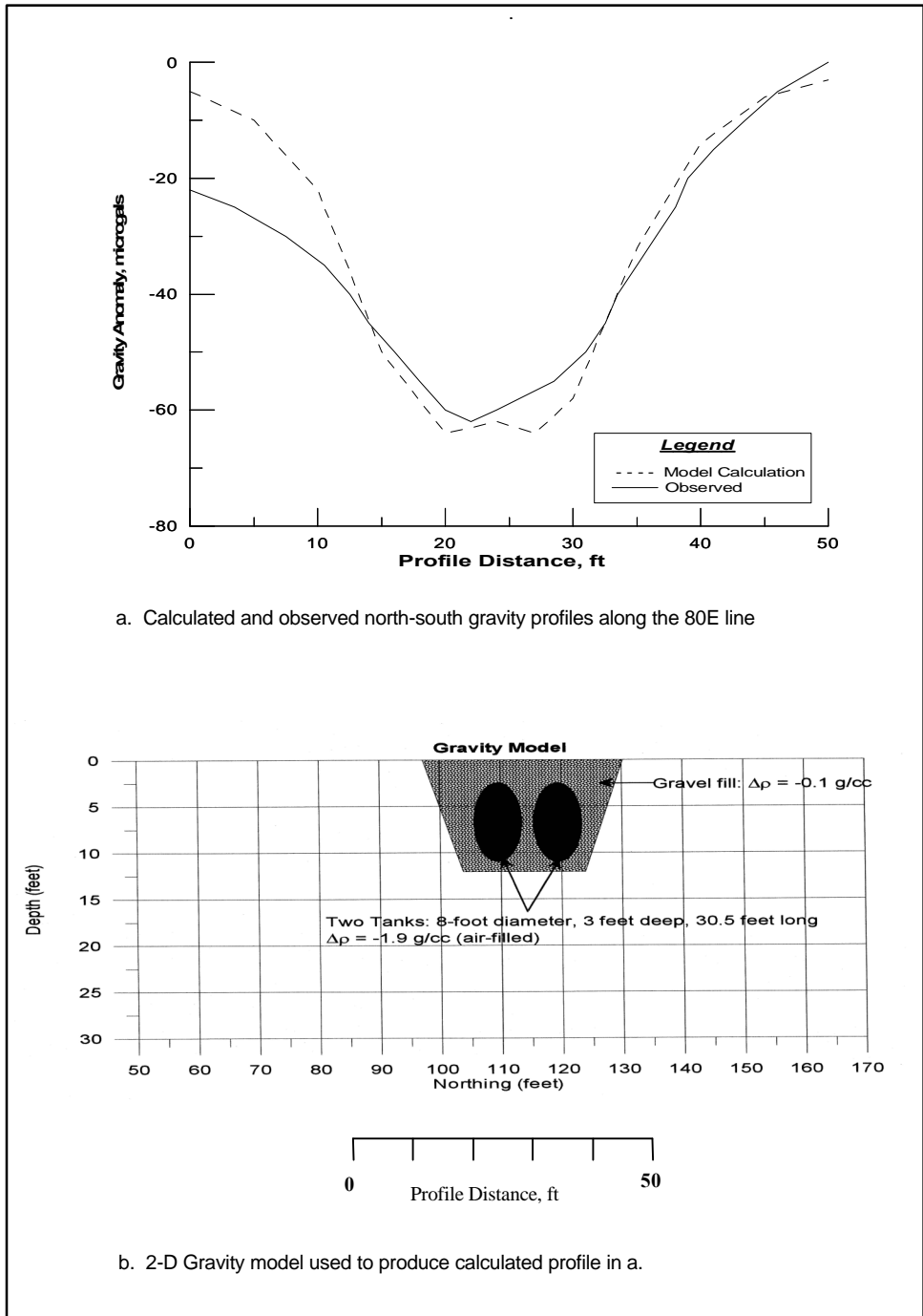


Figure 10. Observed and calculated gravity profiles and 2-D model of UST's and trench

- a. Latitude = 32.306859 deg north.
- b. Longitude = 90.856927 deg west.
- c. Elevation = 60.37 m.

The survey area is  $3 \times 3$  m, and the measurement grid spacing is 0.5 m. The gravimeter was an EDCON Super-G, a modified LaCoste and Romberg Model G gravimeter with force feedback nulling, electronic levels, digital data acquisition, and real-time earth tide, off-level, and temperature corrections. The Super-G is controlled by a palm top computer that stores measurements and has a graphical display of all meter parameters and data as acquired. For this survey, the data acquisition was configured to acquire 15-sec average values, based on one measurement per second. A gravity reading versus time plot displays the data as acquired. At the end of each 15-sec period, the average value is plotted in a second graph. Each station measurement procedure consists of acquiring at least five 15-sec averages.

Station (0,0) is the elevation reference for the survey and was the base station for the gravity measurement program. Also, station (0,0) was assigned the site latitude, and latitude corrections were relative to (0,0). Each loop through the measurement grid (i.e., return to the base station) was made in less than 45 min. Station elevations were determined to an accuracy of better than 0.003 m to ensure gravity elevation corrections to  $\leq 1 \mu\text{Gal}$ . The relative elevation data are given in Table 3, and a contour map for the site is presented in Figure 12. There is a 0.12-m maximum elevation difference over the site.

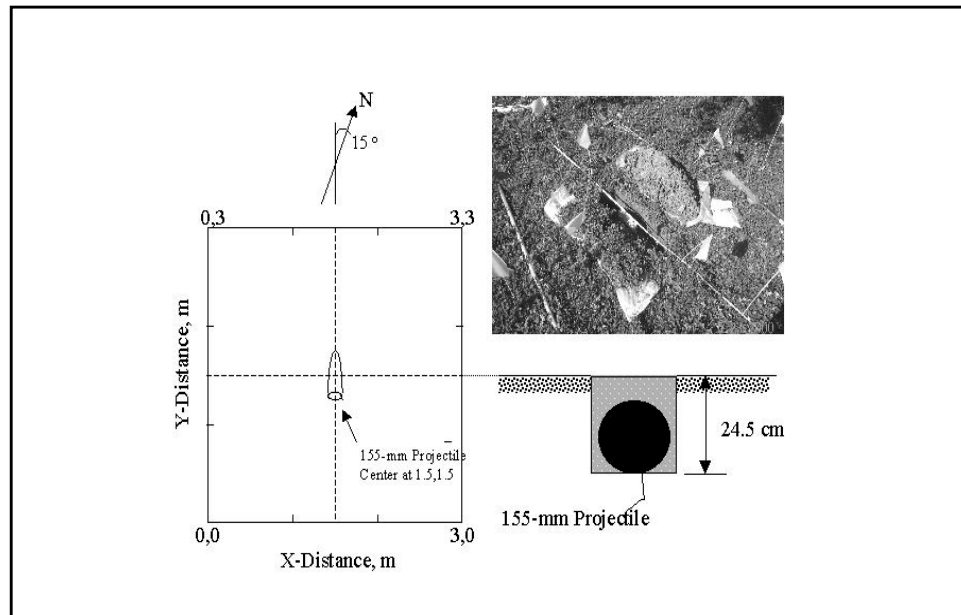


Figure 11. Plan view of survey area, cross section of 155-mm projectile burial, and photograph of the projectile burial

**Table 3**  
**Observed and Corrected Gravity Over 155-mm Projectile Site**

X, m	Y, m	Observed Gravity	Mean St. Dev.	Relative Elevation	Latitude Correction	Free-Air Correction	Bouguer Correction	Bouguer Anomaly	Relative Anomaly
		microgal	microgal	m	microgal	microgal	microgal	microgal	microgal
0	0	59	1.8	0.000	0.00	0.00	0.00	59.0	0.0
0	1	77	1.4	-0.052	-0.73	-15.99	4.31	64.6	5.6
0.5	1	73	1.2	-0.046	-0.73	-14.10	3.81	62.0	3.0
1.5	1	68	2.1	-0.015	-0.73	-4.69	1.27	63.8	4.8
2	1	57	0.7	-0.003	-0.73	-0.93	0.25	55.6	-3.4
2.5	1	61	0.9	-0.003	-0.73	-0.93	0.25	59.6	0.6
3	1	61	1.5	-0.015	-0.73	-4.69	1.27	56.8	-2.2
0	2	85	0.6	-0.085	-1.46	-26.32	7.11	64.3	5.3
0.5	2	73	3.9	-0.076	-1.46	-23.52	6.35	54.4	-4.6
1	2	70	2.6	-0.061	-1.46	-18.82	5.08	54.8	-4.2
1.5	2	71	0.6	-0.052	-1.46	-15.99	4.31	57.9	-1.1
2	2	72	1	-0.049	-1.46	-15.06	4.07	59.5	0.5
2.5	2	71	1.3	-0.043	-1.46	-13.18	3.56	59.9	0.9
3	2	67	3.6	-0.037	-1.46	-11.29	3.05	57.3	-1.7
0	3	79	0.9	-0.104	-2.19	-31.97	8.63	53.5	-5.5
1	3	71	0.7	-0.082	-2.19	-25.40	6.86	50.3	-8.7
2	3	70	1.4	-0.095	-2.19	-29.16	7.87	46.5	-12.5
3	3	61	1.5	-0.040	-2.19	-12.22	3.30	49.9	-9.1
3	0	60	1.6	-0.031	0.00	-9.41	2.54	53.1	-5.9
2	0	53	2.6	0.024	0.00	7.53	-2.03	58.5	-0.5
1	0	62	0.3	-0.003	0.00	-0.93	0.25	61.3	2.3
0	1.5	82	1.7	-0.070	-1.09	-21.63	5.84	65.1	6.1
0.5	1.5	67	1.2	-0.058	-1.09	-17.87	4.82	52.9	-6.1
1	1.5	68	2	-0.043	-1.09	-13.18	3.56	57.3	-1.7
1.5	1.5	72	2.7	-0.037	-1.09	-11.29	3.05	62.7	3.7
2	1.5	57	1.4	-0.021	-1.09	-6.57	1.77	51.1	-7.9
2.5	1.5	56	0.1	-0.015	-1.09	-4.69	1.27	51.5	-7.5
3	1.5	55	0.3	-0.027	-1.09	-8.46	2.28	47.7	-11.3
0	0.5	61	1.9	-0.024	-0.36	-7.53	2.03	55.1	-3.9
0.5	0.5	58	1.7	-0.024	-0.36	-7.53	2.03	52.1	-6.9
1	0.5	56	0.9	-0.015	-0.36	-4.69	1.27	52.2	-6.8
1.5	0.5	52	3	0.000	-0.36	0.00	0.00	51.6	-7.4
2	0.5	48	1.6	0.003	-0.36	0.93	-0.25	48.3	-10.7
2.5	0.5	46	1.8	0.012	-0.36	3.76	-1.02	48.4	-10.6
3	0.5	47	0.9	-0.006	-0.36	-1.88	0.51	45.3	-13.7
2.5	0	49	1.2	0.021	0.00	6.57	-1.77	53.8	-5.2
0	2.5	84	0.8	-0.095	-1.82	-29.16	7.87	60.9	1.9
0.5	2.5	75	0.9	-0.082	-1.82	-25.37	6.85	54.7	-4.3
1	2.5	77	0.5	-0.073	-1.82	-22.56	6.09	58.7	-0.3
1.5	2.5	72	1.3	-0.067	-1.82	-20.71	5.59	55.1	-3.9
2	2.5	77	2.2	-0.064	-1.82	-19.75	5.33	60.8	1.8
2.5	2.5	70	1.3	-0.058	-1.82	-17.87	4.82	55.1	-3.9
3	2.5	63	1.1	-0.030	-1.82	-9.38	2.53	54.3	-4.7
0.5	0	59	1.5	-0.003	0.00	-0.93	0.25	58.3	-0.7
1.5	0	57	1.5	0.008	0.00	2.35	-0.63	58.7	-0.3
2.5	3	70	0.8	-0.061	-2.19	-18.82	5.08	54.1	-4.9
1.5	3	73	0.9	-0.082	-2.19	-25.40	6.86	52.3	-6.7
0.5	3	77	0.9	-0.095	-2.19	-29.16	7.87	53.5	-5.5

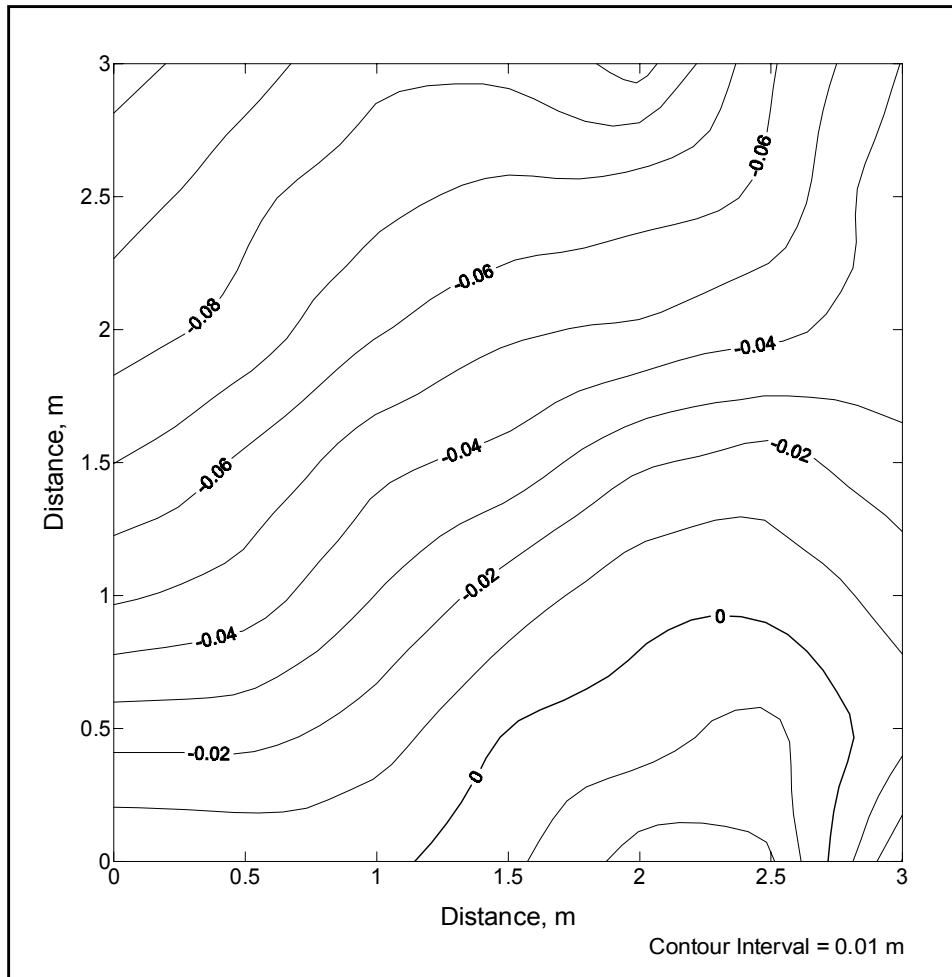


Figure 12. Relative elevation contours of gravity survey site

The survey results, observed gravity data, data corrections, and the relative Bouguer anomaly are in Table 3. For the observed gravity data, all leading numbers that are common to all measurements are suppressed. The Bouguer anomaly value at station (0,0) is subtracted from all Bouguer anomaly values to give the relative anomaly. The mean standard deviation of the measurements ranges from 0.1 to 3.9  $\mu\text{Gal}$ ; the term “mean” applies for stations with multiple occupations (measurement repeats), otherwise it is the standard deviation of the measurements (minimum of five) for one occupation. The mean standard deviation of the measurements for the whole grid is 1.4  $\mu\text{Gal}$ . Figure 13 is a contour plot of the relative anomaly, where the arrow indicates the location, length and orientation of the 155-mm projectile. Relative to the (0,0) gravity reference value, most of the area of the survey grid is negative, except for a small positive area along the western boundary and a closed positive anomaly approximately centered over the 155-mm projectile. The range of relative gravity values over the area is approximately -14 to +6  $\mu\text{Gal}$ , for a maximum variation of 20  $\mu\text{Gal}$ .

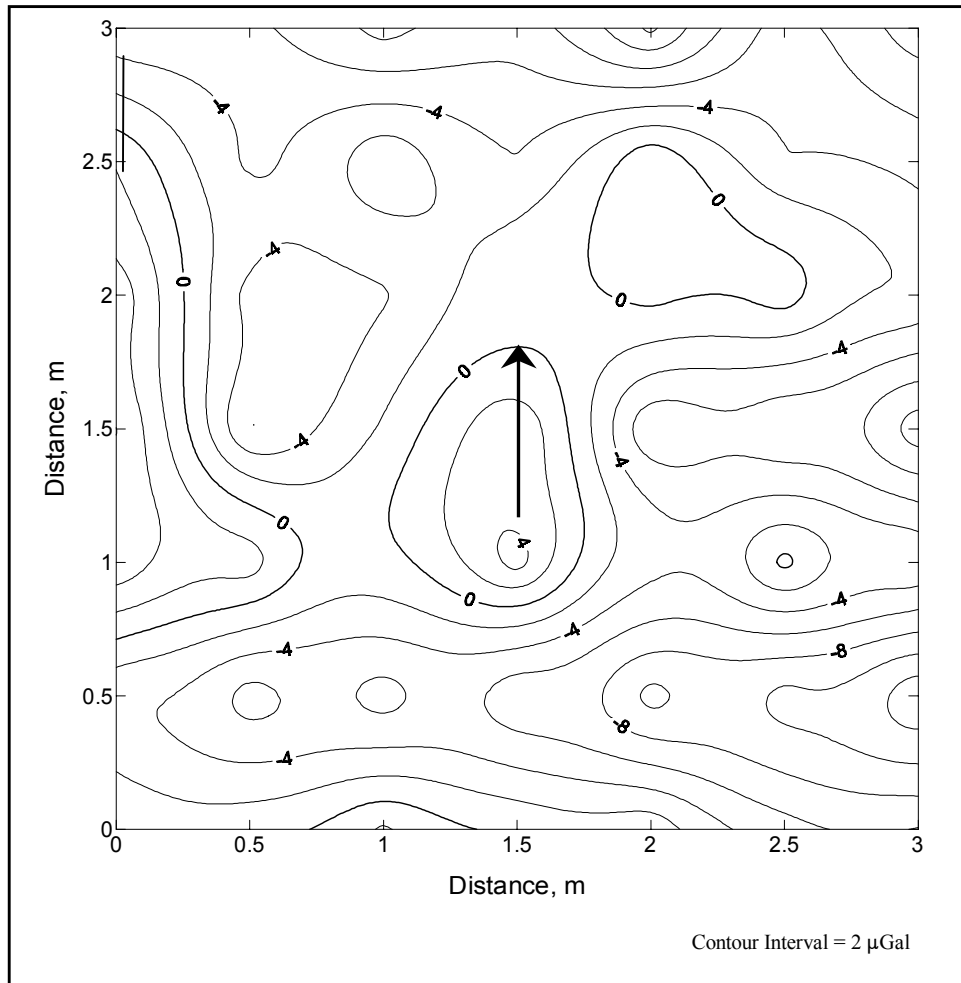


Figure 13. Relative gravity anomaly over survey site; the arrow indicates location, length, and orientation of the 155-mm projectile

## Analysis of Microgravity Survey Results

There is clearly a positive gravity anomaly approximately centered on the buried 155-mm projectile (Figure 13). While there are other closed anomalies in the survey area, the coincidence of the positive anomaly with the location of the projectile is likely not fortuitous. The positive anomaly has approximately the correct spatial wavelength and magnitude, as illustrated in Figure 14, where the measured anomaly is compared to a prolate spheroid model calculation. For the measured anomaly plot in Figure 14 (top), only positive values are shown to facilitate comparison with the calculated anomaly. The measured anomaly has its maximum value near the shank end of the projectile, and the anomaly magnitude and spatial wavelength decrease near the nose end; these features are intuitive for the gravity response of a real projectile buried at very shallow depth ( $\sim 1$ -minor-axis diameter to center). The calculated anomaly for the prolate spheroid model (bottom plot in Figure 14) is centered over the symmetric model (i.e., no differentiation in nose and shank ends for the model).

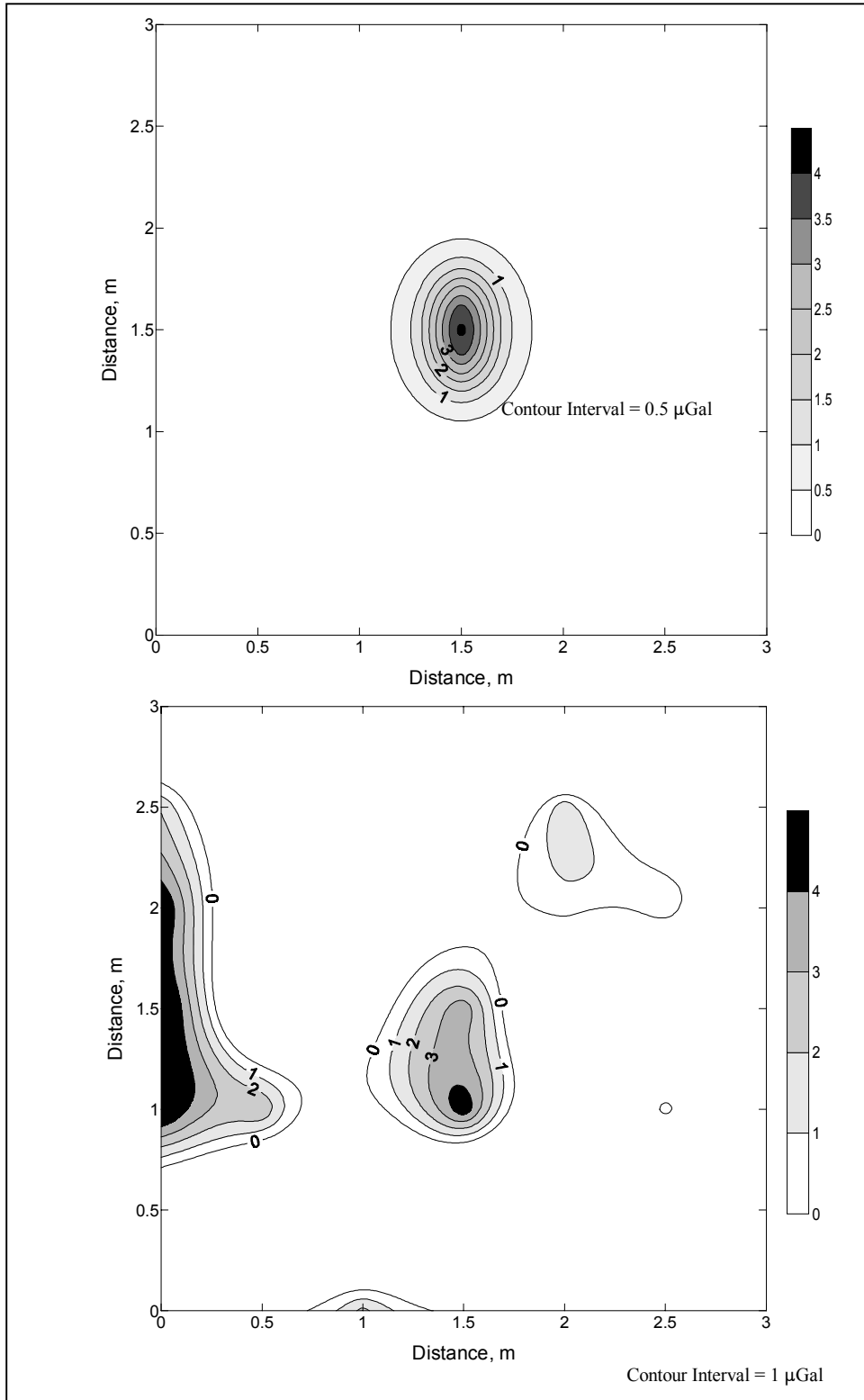


Figure 14. Comparison of measured (top) and calculated (calculated) gravity anomalies

The measured gravity anomaly map in Figure 13 is relative to the point (0,0). The zero level defined by the value at point (0,0) may not be the correct zero level for the survey area. The concept of the proper reference level for the anomaly map is embodied in the definition of the local regional gravity field discussed previously. Clearly, negative anomaly areas surround and are superimposed on the positive anomaly associated with the buried projectile, making it difficult to determine true residual anomaly magnitude and spatial wavelength. Figure 15 shows the east-west gravity anomaly profile along the line  $Y = 1.5$  m (Figure 11) and illustrates three possible regional trends along the profile direction (dashed lines). *The relative anomaly profile as plotted is the residual anomaly for a constant value regional (1)*. Subtracting either of the two nonconstant regional trends (2 or 3) yields two additional possible residual anomaly profiles. The residual anomaly relative to regional 2 or 3 will have greater magnitude and spatial wavelength. Residual anomaly magnitudes, relative to regional 2 and 3, are approximately 5.5 and 8.5  $\mu\text{Gal}$ , respectively; compared to the measured (relative to regional 1) and calculated model values of 3.5 and 5  $\mu\text{Gal}$ , respectively. For regional 2 and 3, the zero level for the anomaly is apparently defined on the east (right) side of the profile, and both residual anomalies have a spatial wavelength of  $\sim 0.4$  m compared to the spheroidal model anomaly spatial wavelength of  $\sim 0.33$  m.

Thus, the microgravity survey results successfully detect a positive anomaly associated with an inert, buried 155-mm projectile. The anomaly locates the projectile (within 0.25 m or better) and indicates the general orientation. Also, due to the very shallow depth of burial, the gravity anomaly reveals further details about the orientation. The maximum of the anomaly is located at the shank end of the projectile; and, not knowing the actual orientation of the projectile, the anomaly could be interpreted in two ways: (1) *a very shallow buried, elongated item* with the maximum indicating the end of the item with greatest mass concentration; (2) an elongated item at arbitrary depth (albeit definitely shallow) that dips to the north (Figure 2). However, the positive anomaly is superimposed on surrounding negative anomalies, making it impossible to determine the true zero level of the anomaly and thus compute excess mass (Equation 17 and associated discussion).

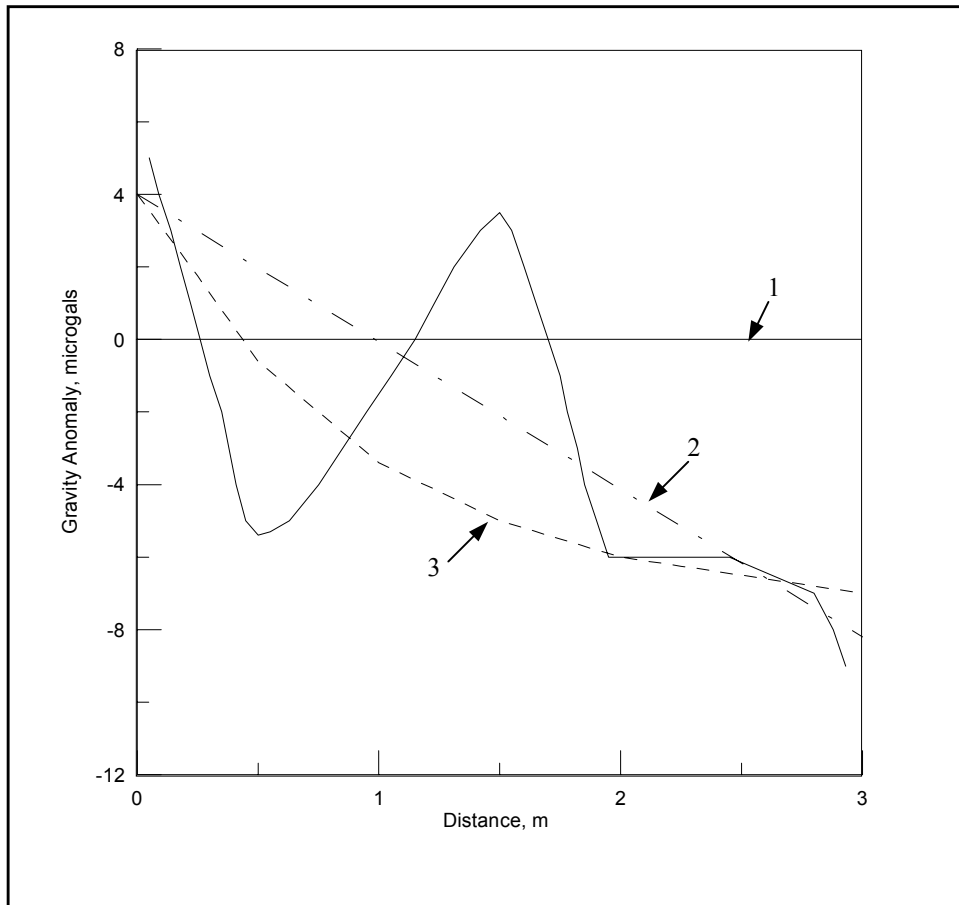


Figure 15. Gravity anomaly profile along the Y = 1.5-m east-west line (from Figure 13), along with three possible regional trends along the line

# 5 Summary and Recommendations

---

## Summary and Conclusions

*A new capability to model the gravity anomaly field on the ground surface of buried spheroidal-shaped objects is developed.* The modeling capability is applicable to predicting the gravity anomalies of objects such as buried UXO (prolate spheroid), land mines (oblate spheroid), underground storage tanks (prolate or oblate), landfills, and other localized features which can be approximated with a spheroidal geometry. The application of the modeling capability discussed in this report is buried UXO detection and discrimination. Specifically, the thrust is to use the modeling capability to assess (1) the detectability of UXO by microgravity surveying and (2) the potential for discrimination.

The gravity anomaly signatures of ordnance items ranging from 105-mm projectiles to 16-in. projectiles and 2,000-lb bombs are modeled. Average lengths, diameters, masses, bulk density, and density contrast are computed for 10 ordnance item types. The density contrasts of the ordnance items are assumed relative to a  $2.0 \text{ g/cm}^3$  soil, and range from  $\sim 1.5 \text{ g/cm}^3$  for large bombs (e.g., 2,000-lb bomb) to  $\sim 5 \text{ g/cm}^3$  for large projectiles (e.g., 16-in. projectile). Gravity anomaly signatures for these ordnance items are examined for maximum value (magnitude) and spatial wavelength to assess detectability. Relative to a nominal detection threshold ( $5 \text{ } \mu\text{Gal}$ ), all the items are detectable at the shallowest depth, i.e., buried horizontally at a depth to center equal to half the diameter or just below the surface. Only five items, 1,000-lb bomb and larger, are detectable at depths  $\sim 0.5 \text{ m}$  or greater, and only the 16-in. projectile is detectable at a depth of 1 m. The gravity anomalies of ordnance items will require measurement spacing of 0.25 to 0.75 m. Considering an optimized survey detection (minimum) threshold ( $2 \text{ } \mu\text{Gal}$ ) will approximately double the predicted detection depths for the ordnance items, but this minimum detection threshold will be difficult to achieve in the presence of geologic background anomalies.

Results of a microgravity survey over a buried 155-mm projectile are presented. A positive gravity anomaly associated with the projectile is detected and the magnitude and spatial wavelength are consistent with spheroidal model predictions. The gravity anomaly also indicates the general orientation of the

projectile. The magnitudes of the measured and predicted anomalies are both  $\sim 4.5 \mu\text{Gal}$  or approximately equal to the nominal detection threshold. The positive anomaly is superimposed on surrounding negative anomalies, and there are other closed anomaly features within the  $3 \times 3\text{-m}$  survey area. One of the additional anomaly features is positive and comparable to the ordnance item anomaly. The measurement spacing for the survey is  $0.5 \text{ m}$ , *which is likely the highest spatial resolution microgravity survey ever conducted*. Background geologic (soil) variation produces gravity anomalies (both positive and negative) at this scale that are comparable in magnitude and spatial wavelength to the buried ordnance item gravity anomalies.

In general, except for the largest ordnance items buried at very shallow depths, microgravity surveying is not a viable technique for detection and discrimination of buried UXO in real world settings.

## Recommendations

Based on the results of predictions of theoretical gravity anomalies with a prolate spheroid modeling program and on a limited field microgravity survey investigation, *it is recommended that microgravimetry not be considered further as a candidate method for UXO detection and discrimination*. The gravity modeling capability developed as a result of this work will be useful as a modeling tool for other environmental geophysics applications, such as underground storage tank detection and condition assessment, landfill investigations, and other detection requirements for localized buried features. The stringent requirements for extremely high resolution microgravity surveying developed as part of the field surveys will be useful for the previously mentioned applications.

# References

---

- Altshuler, Thomas W. (1996). "Shape and orientation effects on magnetic signature prediction for unexploded ordnance," *Proceedings of the UXO Forum 1996*, Williamsburg, VA, 282-291.
- Ander, M.E., Summers, T., and Gruchalla, M.E. (1999). "LaCoste & Romberg gravity meter: System analysis and instrumental errors," *Geophysics* 64(6) 1706-1719.
- Arfken, George. (1985). *Mathematical methods for physicists*. Academic Press, Orlando, FL.
- ASTM. (2000). "Standard guide for using the gravity method for subsurface investigation," D6430-99, Committee D18.01, American Society for Testing and Materials, Philadelphia, PA.
- Barrow, Bruce, Khadr, Nagi, and Nelson, Herbert H. (1996). "Performance of electromagnetic induction sensors for detecting and characterizing UXO," *Proceedings of the UXO Forum 1996*, Williamsburg, VA, 308-314.
- Blakely, Richard J. (1995). *Potential theory in gravity and magnetic applications*. Cambridge University Press, New York.
- Burger, H. Robert. (1992). *Exploration geophysics of the shallow subsurface*. Prentice Hall, Englewood Cliffs, NJ.
- Burr, Arnold P. (1999). Phase IV advanced technology demonstrations at JPG: *Proceedings of the UXO Forum '99*, Atlanta, GA.
- Butler, Dwain K. (1980). Microgravimetric techniques for geotechnical applications: Misc. Paper GL-80-13, U.S. Army Engineer Waterways Experiment Station, Vicksburg, MS.
- \_\_\_\_\_. (1984). "Microgravimetric and gravity gradient techniques for detection of subsurface cavities," *Geophysics*, 49(7), 1084-1096.
- \_\_\_\_\_. (1996). "Microgravity," *The Military Engineer* 88(579), 40-41.

- Butler, Dwain K., Gangi, Anthony F., Wahl, Ronald E., Yule, Donald E., and Barnes, Donald E. (1982). "Analytical and data processing techniques for interpretation of geophysical survey data," Miscellaneous Paper GL-82-16, U.S. Army Engineer Waterways Experiment Station, Vicksburg, MS.
- Butler, Dwain K., Sjostrom, Keith J., and Llopis, Jose L. (1997). "Selected short stories on novel applications of near-surface geophysics," *The Leading Edge*, 16(11), 1593-1600.
- Butler, Dwain K., Cespedes, Ernesto R., Cox, Cary B., and Wolfe, Paul J. (1998). "Multisensor methods for buried unexploded ordnance detection, discrimination, and identification," Technical Report GL-98-10, U.S. Army Engineer Waterways Experiment Station, Vicksburg, MS.
- Gamey, T. J. and Mahler, R. (1999). "A comparison of surface towed and helicopter mounted magnetometer systems for UXO detection," *Proceedings of SAGEEP '99*, 783-792.
- Gamey, T. J., Doll, W. E., Duffy, A., and Millhouse, S. D. (2000). "Evaluation of improved airborne techniques for detection of UXO," *Proc. of SAGEEP '00*, Arlington, VA, 57-66.
- Grant, F. S., and West, G. F. (1965). *Interpretation theory in applied geophysics*. McGraw Hill Book Company, New York.
- Hinze, W. J., Roberts, R. L., and Leap, D. I. (1990). "Combined analysis of gravity and magnetic anomaly data in landfill investigations," *Geotechnical and Environmental Geophysics, Volume II, Environmental and Groundwater*, Society of Exploration Geophysicists, Tulsa, OK, 267-272.
- McDonald, J. R., and Robertson, R. (1996). "Multisensor Towed Array Detection System (MTADS), an automated high-efficiency survey system for characterization of ordnance and explosive waste (OE) sites." *Proceedings of the UXO Forum '96*, Williamsburg, VA, 53-59.
- McFee, John E., and Das, Yogadhis. (1990). "A multipole expansion model for compact ferrous object detection," *Proceedings of the ANTEM Symposium on Antenna Technology and Applied Electromagnetics*. Manitoba, Canada, 633-638.
- MacMillan, William Duncan. (1958). *The theory of the potential*. Dover Publications Inc., New York.
- McNeill, J. D., and Bosnar, Miro. (1996). "Application of time domain electromagnetic techniques to UXO detection," *Proceedings of the UXO Forum 1996*. Williamsburg, VA, 34-42.

- National Research Council. (2000). *Seeing into the earth: Noninvasive characterization of the shallow subsurface for environmental and engineering applications*, National Academy Press, Washington, DC.
- Ramsey, A. S. (1961). *An introduction to the theory of Newtonian attraction*. Cambridge University Press, Cambridge.
- Simms, Janet E., Butler, Dwain K., and Smithhart, Louis B. (2000). "High-resolution, three component magnetic field measurements for UXO model validation and discrimination studies." *Proceedings of the UXO Forum 2000*, Anaheim, CA.
- Sjostrom, Keith J., and Butler, Dwain K. (1996). "Noninvasive weight determination of stockpiled ore through microgravity measurements," Miscellaneous Paper GL-96-24, U.S. Army Engineer Waterways Experiment Station, Vicksburg, MS.
- Snyder, D. D., MacInnes, Scott, Urquhart, Scott, and Zonge, K. L. (2000). "UXO classification using characteristic modes of the broadband electromagnetic induction response." *Proceedings of SAGEEP '00*, Arlington, VA, 747-756.
- USAEC. (1997). "UXO Technology Demonstration Program at Jefferson Proving Ground, Phase III," Report No. SFIM-AEC-ET-CR-97011, U.S. Army Environmental Center, Aberdeen Proving Ground, MD.
- Yule, Don E., Sharp, Michael K., and Butler, Dwain K. (1998). "Microgravity investigations of foundation conditions," *Geophysics*, 63(1), 95-103.

# REPORT DOCUMENTATION PAGE

*Form Approved*  
*OMB No. 0704-0188*

Public reporting burden for this collection of information is estimated to average 1 hour per response, including the time for reviewing instructions, searching existing data sources, gathering and maintaining the data needed, and completing and reviewing the collection of information. Send comments regarding this burden estimate or any other aspect of this collection of information, including suggestions for reducing this burden, to Washington Headquarters Services, Directorate for Information Operations and Reports, 1215 Jefferson Davis Highway, Suite 1204, Arlington, VA 22202-4302, and to the Office of Management and Budget, Paperwork Reduction Project (0704-0188), Washington, DC 20503.

<b>1. AGENCY USE ONLY (Leave blank)</b>	<b>2. REPORT DATE</b> December 2000	<b>3. REPORT TYPE AND DATES COVERED</b> Final report	
<b>4. TITLE AND SUBTITLE</b> Assessment of Microgravimetry for UXO Detection and Discrimination		<b>5. FUNDING NUMBERS</b>	
<b>6. AUTHOR(S)</b> Dwain K. Butler			
<b>7. PERFORMING ORGANIZATION NAME(S) AND ADDRESS(ES)</b> U.S. Army Engineer Research and Development Center Geotechnical and Structures Laboratory 3909 Halls Ferry Road, Vicksburg, MS 39180-6199		<b>8. PERFORMING ORGANIZATION REPORT NUMBER</b> ERDC/GSL TR-00-5	
<b>9. SPONSORING/MONITORING AGENCY NAME(S) AND ADDRESS(ES)</b> Strategic Environmental Research and Development Program U.S. Army Corps of Engineers Washington, DC 20314-1000		<b>10. SPONSORING/MONITORING AGENCY REPORT NUMBER</b>	
<b>11. SUPPLEMENTARY NOTES</b>			
<b>12a. DISTRIBUTION/AVAILABILITY STATEMENT</b> Approved for public release; distribution is unlimited.		<b>12b. DISTRIBUTION CODE</b>	
<b>13. ABSTRACT (Maximum 200 words)</b>  A new capability to model the gravity anomaly field on the ground surface of buried spheroidal-shaped objects is developed. The modeling capability is applicable to predicting the gravity anomalies of objects such as buried UXO (prolate spheroid), land mines (oblate spheroid), underground storage tanks (prolate or oblate), landfills, and other localized features which can be approximated with a spheroidal geometry. The gravity anomaly signatures of ordnance items ranging from 105-mm projectiles to 16-in. projectiles and 2,000-lb bombs are modeled. Average lengths, diameters, masses, bulk density and density contrast are computed for 10 ordnance item types. The density contrasts of the ordnance items are assumed relative to a 2.0 g/cm <sup>3</sup> soil, and range from ~ 1.5 g/cm <sup>3</sup> for large bombs (e.g., 2,000-lb bomb) to ~ 5 g/cm <sup>3</sup> for large projectiles (e.g., 16-in. projectile). Gravity anomaly signatures for these ordnance items are examined for maximum value (magnitude) and spatial wavelength to assess detectability. Relative to a nominal detection threshold (5 µGal), all the items are detectable at the shallowest depth, i.e., buried horizontally at a depth to center equal to half the diameter or just below the surface. Only five items, 1,000-lb bomb and larger, are detectable at depths ~ 0.5 m or greater, and only the 16-in. projectile is detectable at a depth of 1 m. The gravity anomalies of ordnance items will require measurement spacing of 0.25 to 0.75 m. An optimized survey detection (minimum) threshold (2 µGal) will approximately double the predicted detection depths for <span style="float: right;">(Continued)</span>			
<b>14. SUBJECT TERMS</b> Detection Geophysics Microgravimetry		Microgravity Unexploded Ordnance (UXO)	<b>15. NUMBER OF PAGES</b> 43
			<b>16. PRICE CODE</b>
<b>17. SECURITY CLASSIFICATION OF REPORT</b> UNCLASSIFIED	<b>18. SECURITY CLASSIFICATION OF THIS PAGE</b> UNCLASSIFIED	<b>19. SECURITY CLASSIFICATION OF ABSTRACT</b>	<b>20. LIMITATION OF ABSTRACT</b>

### 13. (Concluded).

the ordnance items, but this minimum detection threshold will be difficult to achieve in the presence of geologic background anomalies. Results of a microgravity survey over a buried 155-mm projectile are presented. A positive gravity anomaly associated with the projectile is detected and the magnitude and wavelength are consistent with spheroidal model predictions. The gravity anomaly also indicates the general orientation of the projectile. The magnitudes of the measured and predicted anomalies are both  $\sim 4.5 \mu\text{Gal}$  or approximately equal to the nominal detection threshold. The positive anomaly is superimposed on surrounding negative anomalies, and there are other closed anomaly features within the  $3 \times 3\text{-m}$  survey area. One of the additional anomaly features is positive and comparable to the ordnance item anomaly. The measurement spacing for the survey is 0.5 m, which is likely the highest spatial resolution microgravity survey ever conducted. In general, except for the largest ordnance items buried at very shallow depths, microgravity surveying is not a viable technique for detection and discrimination of buried UXO in real world settings.